GRAVITATIONAL LENS DISCOVERY AND INVESTIGATION USING OPTICAL AND INFRA-RED SURVEYS.

A thesis submitted to the University of Manchester
for the degree of Master of Science by Research
in the Faculty of Engineering and Physical Sciences

2010

By
Hayden Rampadarath
School of Physics and Astronomy
Jodrell Bank Centre for Astrophysics

Contents

Word Count ~ 12000

List of Tables

List of Figures

Abstract

This thesis presents a new method, that combines multi-wavelength optical and infrared surveys to detect gravitational lensed candidates. This method takes advantage of a newly discovered property of gravitational lenses, whereby the separation between the two images decreases from optical to infrared wavelengths. The method was initially tested on simulated gravitational lenses, which indicates that the method is complete for image separations greater than 1 arcsecond, and flux ratios less than 6. However, at higher flux ratios, the method was found to be sensitive to gravitational lenses with large separations. The survey began with 24 896 quasars from the United Kingdom Infrared Telescope Deep Sky Survey (UKIDSS), which was reduced to 461 sources that displayed gravitational lens morphologies within a radius of 3 arcseconds. From the 461 sources, 90 sources with image separations greater than 1 arcsecond and flux ratios less than 15 were selected as possible gravitational lenses with our method. This list of 90 gravitational lens candidates are expected to be observed with the Keck telescope at a later date. Comparisons with known lensing rates from previous gravitational lens surveys, our survey is expected to detect 12-30 new gravitational lenses.

The University of Manchester
Hayden Rampadarath
Master of Science by Research (MSc)
Gravitational Lens Discovery and Investigation using Optical and Infra-Red Surveys
4^{th} September 2010

Declaration

No portion of the work referred to in this thesis has been submitted in support of an application for another degree or qualification of this or any other university or other institution of learning.

Copyright

Acknowledgements

I would like to thank Dr. Neal Jackson for his constant guidance, and support during the course of this project. Many thanks to Dr. Eamonn Kerins for keeping us up to date on the ocial and administrative information, which I mostly would forget. To my fellow MSc students Peter, Gulay, Richard, Dimitrios, Nick, and David for the many discussions, help and overall company during this very intensive year. Thanks also to Sarah, Evan and mark for providing many help and guidance with coding, latex, gnuplot, and general linuxy stu. Finally I would like to say the deepest thanks to my wife, Laura for all her support, trust and for helping me keep my sanity.

This research was supported by the EU Framework 6 Marie Curie Early Stage Training programme under contract number MEST-CT-2005-19669 "ESTRELA".

Hayden Rampadarath
Manchester, September 2010

Science is simply common sense at its best, that is, rigidly accurate in observation, and merciless to fallacy in logic
– Thomas Huxley –

Chapter 1

Introduction

1.1 General Introduction

The deflection of light as it propagates through a gravitational field, is known as gravitational deflection. The amount the light is deflected depends upon the mass (or gravitational potential) of the lensing object. This phenomena, was first considered more than 200 years ago, by Johann Soldner, a German geodesist, mathematician and astronomer, then working at the Berlin Observatory (Soldner 1801). Soldner determined that a light ray close to the solar limb would be deflected by an angle $\sim \alpha = 0.84$ arcseconds. Incidentally, before the completion of General Relativity, Albert Einstein obtained (unaware of Soldner's result), the same value for the deflection angle as Soldner (Einstein 1911; Schneider et al. 2006). Following, the completion of General Relativity, he recalculated the deflection angle and obtained a value twice the original (Einstein 1916, 1922). This was later confirmed in 1919 by Arthur Eddington and his group, to within 20 % during a solar eclipse (Dyson et al. 1920).

Soon after, the lensing effect of stellar mass objects on background stars, was considered by Chwolson (1924) and Einstein (1936). Einstein eventually concluded that "there is no great chance of observing this phenomenon". However, this view was not shared by Fritz Zwicky, who in 1937 suggested that galaxies (then known as "extragalactic nebulae) are much more likely to be gravitationally lensed than stars and that one can use the gravitational lens effect as a "natural telescope (Zwicky 1937a,b). It was not until the discovery of the first gravitational lensed system by Walsh et al. (1979), the quasar QSO 0957+561A,B that the field attracted attention (Narayan & Bartelmann 1996; Wambsganss 1998;

Schneider et al. 2006). Many convincing examples of multiple-imaged quasars are known today, and the list continues to grow.

Previously gravitational lensing by galaxy clusters had only been considered theoretically even before the discovery by Walsh et al. (1979), Narayan & Bartelmann (1996). The subject entered the observational realm with the discovery of giant blue luminous arcs in the galaxy clusters A370 and Cl2244 (Lynds & Petrosian 1986; Soucail et al. 1987). Paczynski (1987) proposed that the arcs are images of background galaxies that have been strongly distorted and elongated by the gravitational lens effect of the foreground cluster. This explanation was confirmed when the first arc redshifts were measured and found to be significantly greater than that of the clusters (Soucail et al. 1988; Fort et al. 1988).

Gravitational lensing manifests itself through a very broad and interesting range of phenomena. Lensing itself has developed into a powerful tool capable of studying a host of important questions in astrophysics. It is divided into three areas; (strong) gravitational lensing (galaxy or galaxy cluster mass lens), weak gravitational lensing (galaxy or galaxy cluster mass lens) and microlensing (stellar mass lens) (Schneider et al. 2006). Where the difference between strong and weak lensing is that strong lensing produces multiple images, unlike weak lensing*. The applications of gravitational lensing may be broadly classified under three categories (Narayan & Bartelmann 1996):

- Objects that are intrinsically too faint or too far (high redshift, z galaxies and quasars) to be observed, are observed due to the magnification effect of lensing. Lenses therefore act as "cosmic telescopes" which allows us to infer source properties far below the resolution limit or sensitivity limit of current observations. However, we do not have the ability to point this telescope at any particular object of interest but we have to work with whatever nature gives us. There have been a number of high redshift galaxies and quasars observed using cosmic telescopes; BRI 0952-0115 at $z = 4.426$ (McMahon et al. 1992), PSS 2322+1944 at $z = 4.12$ (Carilli et al. 2002; Riechers et al. 2008) and SDSS J094604.90+183541.8 at z =4.8 (McGreer et al. 2010),

- As we shall see later, gravitational lensing depends only on the projected,

*A weak lensing effect can be a small deformation of the shape of a cosmic object, or a small modification of its brightness. It is generally more common in nature, as any non-uniform matter distribution between our observing point and distant sources affects the measurable properties of the sources. See Bartelmann & Schneider (2001) for more information

two-dimensional mass distribution of the lens, and is independent of the luminosity, composition or dynamics of the lens. Lensing therefore offers an ideal way to detect and study dark matter in the universe (Treu & Koopmans 2002, 2004; Comerford et al. 2006; Koopmans et al. 2006; Ferreras et al. 2008; Gavazzi et al. 2007; Suyu et al. 2009).

- Many properties of individual lens or samples of lensed objects depends on the age, the scale, and the overall geometry of the universe. The Hubble constant (H_o), the cosmological constant (Λ), and the matter density parameter of the universe (Ω) can be significantly constrained through lensing (Koopmans & the CLASS collaboration 2001; Chae et al. 2004; York et al. 2005; Dobke et al. 2009).

1.2 Importance of Surveys

As discussed in the last section, gravitational lensing is a unique tool for exploring cosmology and the structures of astronomical objects. The well-understood physics of lensing makes it straightforward to use as a cosmological probe (Oguri et al. 2006; Dobke et al. 2009). Moreover, it is the only method that probes distributions of dark matter directly, since gravitational lensing is a purely gravitational phenomenon.

While detailed investigations of single intriguing lensed systems are useful for cosmological and astrophysical applications, for some studies it is essential to do statistical analyses of a complete sample of lenses that are selected from a well-understood source population. For instance, the optical depth for strong lensing, τ_{GL} (i.e the strong lens probability) is sensitive to the cosmological volume element out to moderately high redshift (Figure 1.1). Figure 1.1 shows that for cosmological models with small values of Ω_0 and correspondingly larger values of the cosmological constant, Λ all have much higher values of τ_{GL} at typical quasar redshifts, than a model with $\Omega_0 = 0$, and $\Lambda = 1$ (Turner 1990). Thus gravitational lens statistics can provide valuable constraints on the cosmological constant or more generally, the dark energy density and its equation of state (Turner 1990; Fukugita et al. 1990; Kochanek 1996; Chiba & Yoshii 1999; Mitchell et al. 2005; Oguri et al. 2006).

Strong lensing probabilities at the cluster mass scale are able to probe both the abundance and mass distribution of clusters (Narayan & White 1988; Maoz

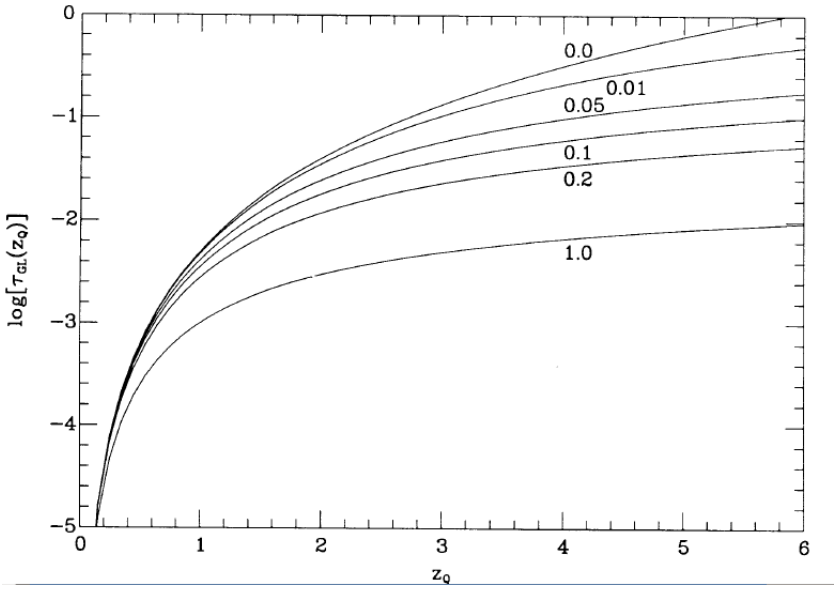

Figure 1.1: The gravitational lensing optical depth, τ_{GL} as a function of source redshift, z_Q for six spatially flat (k = 0) cosmological models. The curves are labeled by their assumed values of Ω_0 (Turner 1990)

et al. 1997). The lensed image separation distribution from galaxy to cluster mass scales can be used to study baryon cooling in dark halos (Kochanek & White 2001) and the connection between galaxy luminosities and masses of host halos (Oguri 2006).

A statistical sample is important not only for studies of lensing rates but also for interpreting the results of individual lens modelling. It has been argued that lensing objects may be more or less typical in their shapes, orientations (Hennawi et al. 2006) and environments (Oguri et al. 2005) because of strong dependencies of lensing probabilities on these quantities. Therefore, proper account must be taken of lensing biases to make a fair comparison between theory and observed results, which can only be accomplished for a well-defined statistical lens sample. A similar argument holds for constraints from stacked samples of strong lenses, including the structure and evolution of early-type galaxies (Treu & Koopmans 2004; Rusin & Kochanek 2005) and the fraction of substructures in lens galaxies (Dalal & Kochanek 2002).

Another powerful application of gravitational lens surveys, is the determination of the Hubble constant (Refsdal 1964; Saha et al. 2006; Oguri 2007; Suyu et al. 2010). It has been known for some years that time delays between multiple images of certain strong lensing systems allows for constraints on the Hubble

constant (H_0) (Refsdal 1964) due to the dependence of the time delay scaling on this parameter. The constraints on H_0 by means of strong lensing time delays have historically had mixed success, mainly due to its degeneracy with the matter density profile of the lensing galaxy (e.g. Falco et al. (1985); Gorenstein et al. (1988); Corless et al. (2008)). This method was successfully applied by Saha et al. (2006), who combined 10 lensed quasar systems to constrain H_0. They obtained a value of $72 \pm 8\ km^{-1}\,Mpc^{-1}$ for H_0, which is in agreement with the value obtained with Cepheid variables ($73 \pm 4\ km^{-1}\,Mpc^{-1}$, Riess et al. (2005)). More recently Suyu et al. (2010) obtained a value of $70.6 \pm 3.1\ km^{-1}\,Mpc^{-1}$ for H_0 from the strong gravitational lens system B1608+656.

To date more than 100 gravitational lensed systems are now known in which a background galaxy or quasar is multiply imaged by the action of a foreground galaxy (Jackson et al. 2008, 2009), most of which were discovered by by investigation of quasars from the Sloan Digital Sky Survey (SDSS) quasar list (Schneider et al. 2007). The largest survey is the Sloan Lens ACS survey (SLACS) (Bolton et al. 2006), with 60 lensed systems and the SDSS Quasar Lens Search (SQLS) (Oguri et al. 2006; Inada et al. 2010), with 36 newly discovered lenses. There have also been a few searches in the radio regime such as the Cosmic Lens All-Sky Survey (CLASS) and the Jodrell/VLA Astrometric Survey (JVAS) which are surveys of flat-spectrum radio sources designed to identify gravitational lensed candidates (Myers et al. 2003; Browne et al. 2003). Together they discovered 22 lenses. In general, all gravitational lensed surveys can be separated into either source based surveys (Myers et al. 2003; Oguri et al. 2006) or lens galaxies based surveys (Bolton et al. 2006). This will be treated in more detail in Chapter 3.

1.3 Objectives and Thesis Outline

The SDSS (York et al. 2000a) is a very important resource in discovering lensed systems, due to its wide-area sky coverage and consequent large number of observed quasars. The Sixth Data Release of the SDSS (DR6,Adelman-McCarthy et al. (2008b)), has increased the total number of quasars to over 120,000. The typical lensing rates (e.g. Turner et al. (1984)), are expected to be between 0.1 % and 1%, which would be expected to yield more than 1000 gravitational lenses, from the DR6.

Unfortunately, many of these lenses will have relatively small separations, as

it is much more difficult to carry out optical surveys since the high resolution needed to separate the components of a lensed system is not easily available (Jackson et al. 2008, 2009). High-resolution searches with radio interferometers (such as CLASS) reveal a median separation of between 1 and 1.5 arcsec, and substantial numbers with separations smaller than 1 arcsec. Although the SDSS covers a large fraction of the sky to a faint limiting magnitude (r $\sim$ 22), the PSF width of the images is $\sim$ 1.4 arcsec (York et al. 2000a).

More recently the UKIRT Deep Sky Survey (UKIDSS, Lawrence et al. (2007)) has become available. The UKIDSS Large Area Survey (ULAS) covers just over 1000 square degrees to a depth of K=18.4 (corresponding to R $\sim$ 24 for a typical elliptical galaxy at z = 0.3) and, importantly, has a median seeing of 0.8 arcsec. UKIDSS uses the UKIRT Wide Field Camera (WFCAM; (Casali et al. 2007)). Details are given in Chapter 4. Recently, Jackson et al. (2008, 2009) used the UKIDSS in combination with SDSS observations to detect two new gravitational lenses (ULAS J234311.9-005034 and ULAS J082016.1+081216). This study, Major UKIDSS-SDSS Cosmic Lens Survey, (MUSCLES) aims to discover lenses difficult for or inaccessible to the SQLS due to small separation, high flux ratio or a combination of the two. During their study Jackson et al. (2009) discovered that the separation between the two lensed images (A and B) of ULAS J082016.1+081216, decreases from optical to infra-red (Figure 1.2). They explained that this occurs when a relatively red lens galaxy is located between two blue quasar images, and close to the fainter quasar image (Jackson et al. 2009). As the wavelength increases the galaxy becomes brighter, while the brightness of the quasar image decrease, giving the impression that the position of B is moving towards to A. If indeed all optical lensed systems do follow this trend, it can prove to be a very effective and efficient method to reduce the size of a large parent population of candidate gravitational lenses.

The main aim of this thesis is to test the effectiveness of this discovered property as a selection criteria for gravitational lenses. A combination of SDSS and UKIDSS observations are used, along with simulated lensed systems to test the survey's completeness (i.e. false negative rate). However, this research is only intended to produce a list of gravitational lens candidates from a much larger parent population, via this method. The final list of lensed candidates, will be submitted to the Keck telescope [†], for observation on September 15th,

[†]http://keckobservatory.org/

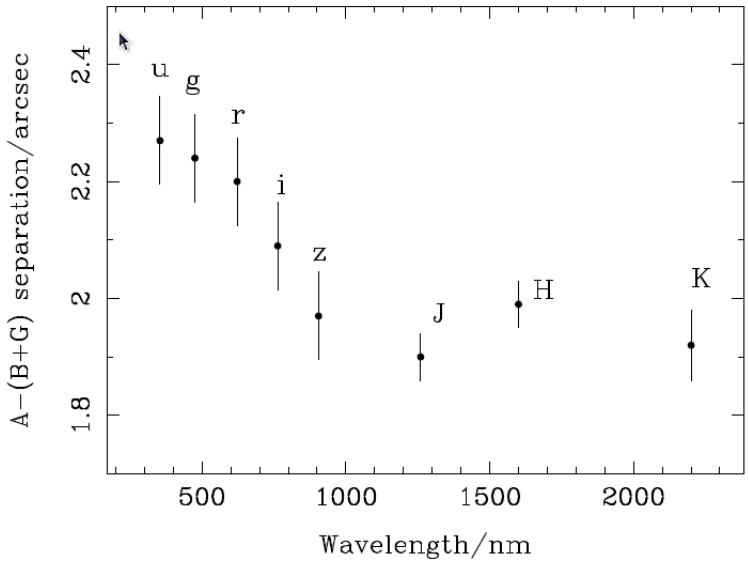

Figure 1.2: Separation of the primary (A) and secondary (B+G) components for the lensed system ULAS J082016.1+081216, in the filters ugrizJHK from SDSS and UKIDSS, against wavelength Jackson et al. (2009).

2010.

1.3.1 Thesis Outline

§ 1 **This introduction**

§ 2 **Basic Theories**
This chapter will introduce the basic theories associated with gravitational lenses, and set the theoretical basis for the rest of the thesis.

§ 3 **Gravitational lens surveys**
This chapter is devoted to the discussion and description of the major gravitational lens surveys.

§ 4 **Sample Selection and Simulations**
This chapter will, in detail describe the parent population and the reduction of the candidates via the selection criteria used in this project, which involves a 4-step procedure. Simulations used to test this selection criteria will also be described.

§ 5 **Results**
The final list of "possible gravitational lensed candidates" will be presented.

§ 6 **Discussion**

The final list of candidates will be compared to the results of the simulations, and with previous gravitational lensed surveys.

§ 7 **Summary**

A summary of the project, and its results will be presented.

Chapter 2

Basic Theories

Please note that most of the information within this section has been obtained from Narayan & Bartelmann (1996); Wambsganss (1998); Schneider et al. (2006), unless otherwise stated

2.1 Lens Equation and Geometry

Figure 2.1, shows the typical lensing geometry where the light from the source, S is deflected by an angle, α, by a lens, L of mass, M. α is known as the *Einstein deflection angle*, and is given by

$$\alpha = 4GM/c^2b, \tag{2.1}$$

where b is the impact parameter. Simple geometry gives us

$$\beta D_S + \alpha D_{LS} = \theta D_S, \tag{2.2}$$

which is rearranged to give

$$\beta - \theta = \alpha D_{LS}/D_S = \hat{\alpha} \tag{2.3}$$

Equation 2.3 is known as the *lens equation*, where D_S, D_L and D_{LS} are the angular distances to the source, the lens and between the source and the lens*. The source is located at θ and in the absence of a lens the source would have been seen at position β. In the last step we define the *scaled deflection angle*, $\hat{\alpha}$.

*note that for cosmological distances in general $D_{LS} \neq D_S - D_L$

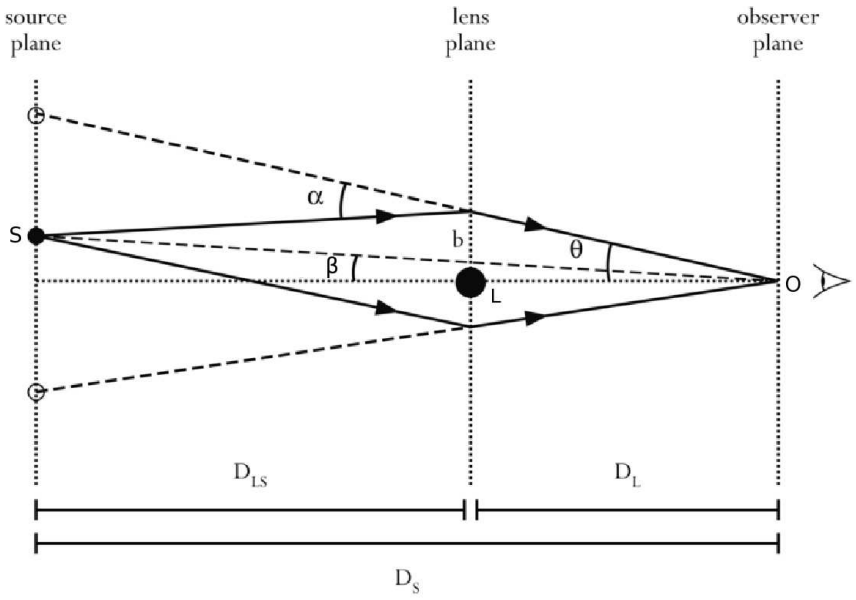

Figure 2.1: Lensing Geometry. *Courtesy Wikipedia*

2.2 Einstein Radius

For a point lens of mass, M, the deflection angle, α is given by Equation 1, substituting into Equation 3 and from Figure 2.1, $b = \theta D_L$ we get,

$$\beta = \theta - \frac{4GM}{c^2\theta}\frac{D_{LS}}{D_S D_L} \tag{2.4}$$

Due to rotational symmetry of the lens system, a source which lies on the optical axis ($\beta = 0$) is imaged as a ring (Narayan & Bartelmann 1996). Setting $\beta = 0$, in Equation 4 we obtain

$$\theta_E = \sqrt{\frac{4GM}{c^2}\frac{D_{LS}}{D_S D_L}} \tag{2.5}$$

This is known as the *Angular Einstein radius*, and the physical Einstein radius is, $R_E = \theta_E D_L$. Figure 2.2 illustrates this situation; the Einstein radius is a very important parameter as it provides a natural angular scale to describe the lensing geometry. Generally, sources which are closer than about θ_E to the optic axis experience strong lensing in the sense that they are significantly magnified, whereas sources which are located well outside θ_E are magnified very little. In many lens models, the Einstein ring also represents roughly the boundary between source positions that are multiply-imaged and those that are only singly-imaged.

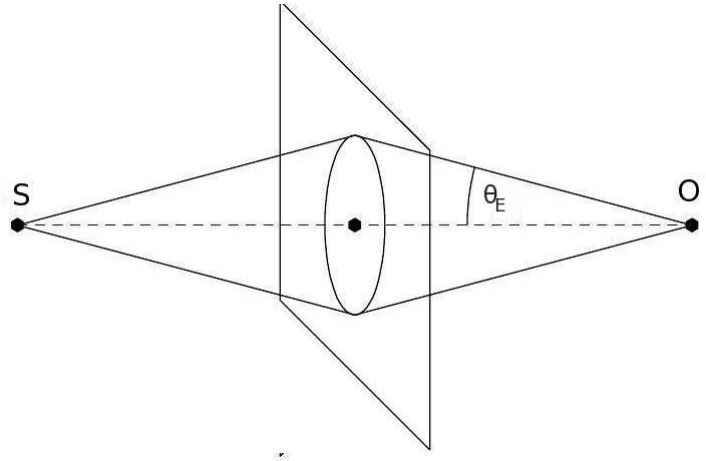

Figure 2.2: A source S on the optical axis ($\beta = 0$) of a symmetric lens, is imaged as a ring with a angular radius given by the Einstein radius, θ_E (Narayan & Bartelmann 1996)

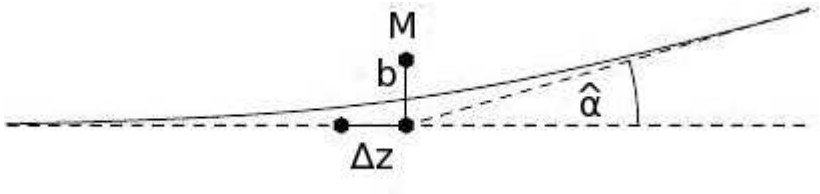

Figure 2.3: The unperturbed ray passes the mass at impact parameter b and is deflected by $\hat{\alpha}$. Most of the deflection occurs within $\triangle z \sim \pm b$ of the point of closest approach (Narayan & Bartelmann 1996).

To give illustrative examples, consider lensing by a star in a the Galaxy with a mass, $M \sim M_\odot$ and $D \sim 10$ kpc, and lensing by a galaxy at a cosological distance of $D \sim 1$ Gpc and $M \sim 10^{11}\, M_\odot$. The corresponding Einstein radii are:

$$\theta_e = (0.9mas)(\frac{M}{M_\odot})^{1/2}(\frac{D}{10kpc})^{1/2}, \tag{2.6}$$

$$\theta_e = (0.9'')(\frac{M}{10^{11}M_\odot})^{1/2}(\frac{D}{Gpc})^{1/2}, \tag{2.7}$$

2.3 Critical Surface Density

Figure 2.3 demonstrates that most of the light deflection occurs within $\triangle z \sim \pm b$ of the point of closest approach between the light ray and the point mass.

Since $\triangle z$ is typically much smaller than the distances between the observer and lens (D_L) and between lens and source (D_{LS}), the lens can be considered thin compared to the total extent of the light path. The mass distribution of the lens can be projected along the line of sight and replaced by a two dimensional surface mass density distribution $\Sigma(\overrightarrow{b})$,

$$\Sigma(\overrightarrow{b}) = \int \rho(\overrightarrow{b}, z)dz \tag{2.8}$$

From equations 2.1-2.3, and 2.8, with the definition of the impact parameter, b we obtain the *critical surface mass density*, Σ_{crit} which is defined as

$$\Sigma_{crit} = \frac{c^2}{4\pi G}\frac{D_S}{D_L D_{LS}}, \tag{2.9}$$

The deflection angle for such a mass distribution can then be expressed as

$$\hat{\alpha}(b) = \frac{\Sigma}{\Sigma_{crit}}\theta \tag{2.10}$$

For an arbitrary mass distribution, the condition $\Sigma > \Sigma_{crit}$ produces multiple images. In general, Σ_{crit} is a characteristic value for the surface mass density is the dividing line between 'weak' and 'strong' lenses.

2.4 Image Positions

From equations 2.1 - 2.5, the following equation can be derived,

$$\theta^2 - \beta\theta + \theta_E^2 = 0 \tag{2.11}$$

which is another form of the *lens equation*, which has 2 solutions for the image positions,

$$\theta_\pm = 1/2[\beta_\pm(\beta^2 + 4\theta_E^2)^{1/2}] \tag{2.12}$$

Any source is imaged twice by a point mass lens. The two images are on either side of the lens, with one image inside the Einstein ring and the other outside. As the source moves away from the lens (i.e. as β increases), one of the images approaches the lens and becomes very faint, while the other image approaches closer to the true position of the source and tends toward a magnification of unity.

Chapter 3

Gravitational lens surveys

3.1 Survey Mechanics

As discussed in section 1.2 gravitational lens surveys have important applications and implications on cosmological and astrophysical studies. In general there are two main approaches to search for gravitational lenses; either you start with a list of potentially lensed sources (Myers et al. 2003; Oguri et al. 2006) or a list of potential lens galaxies (Bolton et al. 2006).

Most lens surveys have taken the lensed source approach, since depending on the observational method, the required number of targets to be surveyed can be considerably less, and are also cosmologically significant *. For a non-evolving population of lenses in a flat cosmological model the number of lensed sources scales with the volume between the observer and the source D_S^3 (Schneider et al. 2006).

This is basically a statement about the relative surface densities of candidate sources and lenses (Schneider et al. 2006). A typical lens is a galaxy with an Einstein radius of approximately $b \simeq 1.0''$, and hence has a cross section of order πb^2. A search for N lenses of this cross section, would discover $N\pi b^2 \Sigma_{source}$ lenses, where Σ_{source} is the surface density of detectable sources. Similarly, if you search N sources for a lens galaxy, $N\pi b^2 \Sigma_{lens}$ lenses would be found, where Σ_{lens} is the surface density of lens galaxies. Since the surface density of massive galaxies is significantly higher than the surface density of easily detectable higher redshift sources ($\Sigma_{lens} \gg \Sigma_{source}$), one would require an examination of fewer

*i.e. they generally are at high mean redshifts, and can be used to determine cosmological parameters

sources than lens galaxies to find the same number of lensed systems (Schneider et al. 2006).

The majority of source-based lens surveys have focused on either optical quasars or radio sources, since they are source populations known to lie at relatively high redshift ($z_s \sim 1$) and are easily detected even with an intervening lens galaxy (Schneider et al. 2006). Optical surveys target quasars, as they sufficiently bright to allow the redshift and magnitude distributions to be accurately determined. Other source types are not bright enough for redshift determination, and as a result are not targeted. However, they have the disadvantage in that, the bright sources generally mask the lens galaxy and the selection process is affected by the light from the lens galaxy and dust reddening (Schneider et al. 2006; Oguri et al. 2006). The SQLS (Oguri et al. 2006) is the most recent and currently the largest source-based optical survey.

Surveys of radio sources either search for steep spectrum sources or flat spectrum sources. While most of the lensed radio sources are produced by extended, steep spectrum sources their complex intrinsic structures make follow up observations very difficult (Kochanek & Lawrence 1990; Schneider et al. 2006). On the other hand, surveys of flat spectrum radio sources, such as the CLASS survey (Myers et al. 2003; Browne et al. 2003) have the advantage that the follow up observations are relatively simple since most unlensed flat spectrum sources are (nearly) point sources Myers et al. (2003); Browne et al. (2003). The main disadvantage with these radio sources, is that because the source structure is relatively simple they provide fewer constraints on mass models than the steep spectrum lenses (Schneider et al. 2006). Another problem is that most radio sources tend to be faint in the optical bands, making it difficult to determine their redshifts (Schneider et al. 2006).

The number of targets to be surveyed are generally much more for lens-based surveys, however they currently account for more than half of the known galaxy-mass lenses (SLACS, Bolton et al. (2006); Treu et al. (2006)). Lensed systems found by searching for galaxies that have lensed a background source, do not have much cosmological significance (Schneider et al. 2006). This is because the cosmological dependence enters only through the distance ratios, D_{ds}/D_s, and precise knowledge of the source redshift distribution is required. However surveys such as SLACS may provide some cosmological significance, since there are multiple sources at different redshifts. In general, lenses found in this manner

are very useful for many other projects such as mass distributions (both baryonic and non-baryonic), galaxy evolution, etc (Rusin et al. 2003; Bolton et al. 2006; Treu et al. 2006; Gavazzi et al. 2007; Ferreras et al. 2008).

Recently there has been the development of a third approach to search for galaxy-scale lenses. Although the SDSS is a wide-field survey, len surveys such as SQLS and SLACS use the individual catalogues (spectroscopic, DR6 etc) to find potential source quasars or lens galaxies. Surveys such as the Canada-France-Hawaii Legacy Survey (CFHTLS) Strong Lensing Legacy Survey (SL2S, Cabanac et al. (2007)), and the Hubble Space Telescope COSMOS lens survey (HSTCLS) (Faure et al. 2008), search for gravitational lenses within wide-field images of $\sim$ 1-2 degrees squared of sky. These wide-field images contains a large number of sources and allows one to identify gravitational lensed sources with multiple lensed sources and massive galaxies with arcs (Cabanac et al. 2007; Faure et al. 2008).

As we shall see in the following sections, all gravitational lens surveys start with a large parent population of tens of thousands of sources (or lens galaxies). Most of these sources are not gravitational lenses, as the parent population are mostly taken from quasar or galaxy catalogues (e.g. SDSS). Thus the parent population must be efficiently reduced to only those sources that present the highest probability of being gravitationally lensed. This reduction must be such that the survey is both complete (i.e. no false negatives, or rejection of actual lenses) and reliable (i.e. no false positives detected). Generally the completeness and reliability of a survey are described within certain parameter space (i.e. flux ratio, redshift, image separation etc.).

To date there have been more than 100 galaxy-scale lenses discovered from optical quasars, radio sources and galaxy lenses (Marshall et al. 2009). The discovery methods are generally a combination of serendipitous discovery and a host of systematic search techniques. These techniques include; visual inspection of deep optical imaging obtained with the Hubble Space Telescope (HST; e.g., Hogg et al. (1996); Zepf et al. (1997); Ratnatunga et al. (1999); Fassnacht et al. (2004); Moustakas et al. (2007)), targeted imaging of the population of potentially lensed quasars or radio sources (e.g., Myers et al. (2003); Browne et al. (2003); Oguri et al. (2004); Pindor et al. (2006)), and follow-up of systems for which optical spectroscopy revealed anomalous emission lines (e.g., Warren et al. (1996); Bolton et al. (2004); Willis et al. (2006)). Further techniques using time-domain

information have also been proposed as efficient lens finders (e.g. Pindor (2005); Kochanek et al. (2006)).

The following sections will discuss the different types of lens surveys that have been most successful.

3.2 Lens-Based Surveys

3.2.1 The Sloan Lens ACS (SLACS) Survey

The SLACS survey (Bolton et al. 2006; Treu et al. 2006; Koopmans et al. 2006; Gavazzi et al. 2007; Bolton et al. 2008a; Gavazzi et al. 2008; Bolton et al. 2008b; Treu et al. 2009; Auger et al. 2009), which began in March 2005, is currently the largest lens based survey. Its main aim was to discover a very large sample of new early-type strong gravitational lenses that are suitable for detailed photometric and dynamical study and to use gravitational lensing as a probe of early-type galaxy structure. The SLACS utilized the method described by Bolton et al. (2004), which selected candidate galaxy-scale gravitational lens systems from the Sloan Digital Sky Survey (SDSS) spectroscopic database on the basis of multiple higher redshift emission lines in the spectrum of lower redshift target galaxies.

The idea behind this is that a massive foreground galaxy should act as an effective gravitational lens of any object positioned sufficiently far behind it and at small enough impact parameter, b. Any emission features from such lensed objects should be detectable in the spectrum of the foreground galaxy (Bolton et al. 2004). Therefore, by searching for discrepant emission features in galaxy spectrum one can potentially discover a sample of gravitational lensed systems that would not be discovered with broadband imaging searches due to the faintness of the source relative to the lens. This idea is not unique to the SLACS survey, and has previously been a very successful method to detect gravitational lens; such as the lensed quasars 2237+0305 (Huchra et al. 1985), the lensed Lyα emitting galaxy 0047-2808 (Warren et al. 1996, 1998, 1999), and SDSS J0903+5028 (Johnston et al. 2003). To get an idea as to the type of "discrepant emission features in galaxy spectra" that are looked for, figure 3.1 shows the spectrum of SDSS J0903+5028 (Johnston et al. 2003). The SDSS spectrum, shows absorption features of an early-type galaxy at redshift, z = 0.388 (e.g., the Ca H and K lines at 5463 and 5510 Å), with quasar CIV emission lines corresponding to a redshift,

z = 3.584.

All sources from the SDSS spectroscopic database that showed these discrepant emission features in the galaxy spectrum, were selected as promising lens candidates[†] for follow up optical observations, using the Advanced Camera for Surveys (ACS) aboard the *Hubble Space Telescope (HST)*. Here detailed measurements of photometric and morphological parameters of the possible lensing galaxies, with which to constrain gravitational lens models were made (Bolton et al. 2004, 2006). 131 promising candidates were selected via the spectroscopic method, and observed with the ACS, of which a total of 70 strong gravitational lenses and a further 19 possible gravitational lenses were confirmed giving a success rate of $\sim 68\%$ (Bolton et al. 2008a). The HST images allowed a measurement of the Einstein radii, which in combination with the redshifts from the SDSS gave direct measurements of the enclosed masses of the lens galaxies (Bolton et al. 2006; Treu et al. 2006). Figure 3.2 shows some of the more impressive lenses discovered by the survey, which has either full or partial Einstein rings.

Although the targeted lens population of SLACS do not have a lot of cosmological implications (i.e they cannot be used to determine cosmological parameters), the survey did obtain some very important results related to the structure and formation of early-type galaxies. For more detailed information please see Bolton et al. (2004, 2006); Treu et al. (2006); Koopmans et al. (2006); Gavazzi et al. (2007); Bolton et al. (2008a); Gavazzi et al. (2008); Bolton et al. (2008b); Treu et al. (2009); Auger et al. (2009):

- SLACS lenses appear in every respect to be just like other "early-type" (i.e., elliptical and lenticular) galaxies in both internal properties and distribution of environments, and the results of the SLACS survey can therefore be generalized to galaxies that do not act as lenses.

- The radial mass density profile of the SLACS lenses is inconsistent with a model wherein the optical light traces mass.

- This radial mass density profile is approximately "isothermal" (density proportional to the inverse square of radius in three dimensions), a result that is found through both self-consistent lensing and dynamical modeling and through simple dimensional analysis.

[†]sources that have a high probability of being a gravitational lensed system

- With regards to the previous results, this profile seems not to have evolved significantly since redshift z=1.
- This mass-density profile slope has a very small but non-zero intrinsic scatter that does not appear to be significantly correlated with any other observable quantity, with the possible exception of a marginally steeper profile for "satellite" galaxies as compared to "central" galaxies.
- SLACS lenses define a "fundamental plane" (FP)[‡] relation that is consistent with the FP of galaxies in the nearby universe, corrected for luminosity evolution.
- The "tilt" of the SLACS FP is due entirely to a variation in total (luminous plus dark) mass-to-light ratio with mass, and not to variations in mass-dynamical structure with mass.
- The projected position angles of mass and light ellipsoids in the SLACS lenses are well aligned with one another.
- The average mass density profile of SLACS lenses as determined from their combined weak-lensing signal is consistent with a continuation of their strong-lensing isothermal profiles from a few kiloparsecs out to a few hundreds of kiloparsecs.

3.3 Source-Based Surveys

3.3.1 The SDSS Quasar Lens Search (SQLS)

Like the SLACS survey, the SDSS Quasar Lens Search (SQLS; Oguri et al. (2006); Inada et al. (2008); Oguri et al. (2008); Inada et al. (2010)) utilized the large homogeneous data of the Sloan Digital Sky Survey (SDSS;York et al. (2000b)). The SQLS is an ongoing project which aims to construct a large statistical sample of lensed quasars that can be used as a cosmological probe, from a sample of spectroscopically confirmed SDSS quasars (Schneider et al. 2005, 2007). To date the SQLS have discovered 11 lensed quasars (Inada et al. 2008) from the SDSS Data

[‡]The fundamental plane is a tight corelation between the effective radius R_e, mean surface brightness μ_e and central velocity dispersion σ_c of early-type galaxies. Discovered by (Djorgovski & Davis 1987; Dressler 1987)

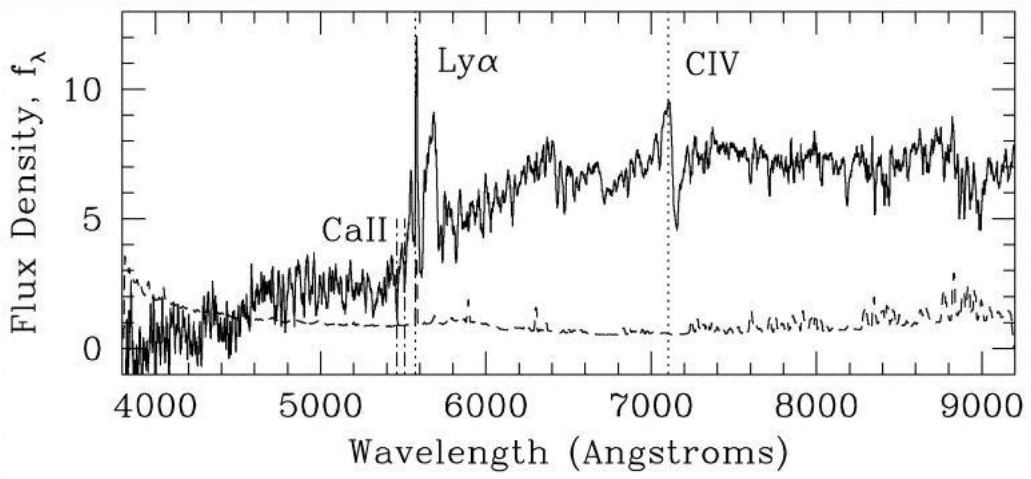

Figure 3.1: SDSS spectrum of SDSS J0903+5028. The error spectrum is given by the dashed line. Dotted lines mark the centers of Lyα and CIV emission for z = 3.584. The flux units are $10^{-17}\, ergs\, s^{-1} cm^{-2}\, \text{Å}^{-1}$ (Johnston et al. 2003).

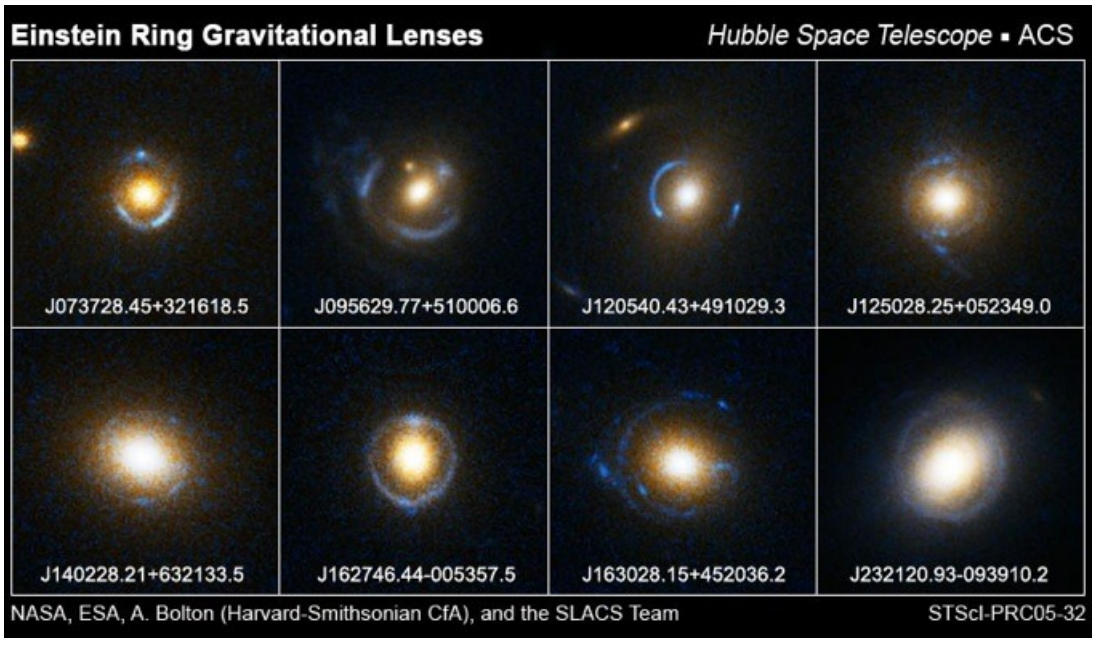

Figure 3.2: Image displaying Einstein rings for 8 of the 70 gravitational lens discovered by the SLACS survey. *Image Courtesy: www.slacs.org/.*

Release 3 (DR3; Schneider et al. (2005)) and 36 lensed quasars (Inada et al. 2010) from the SDSS Data Release 5 (DR5; Schneider et al. (2007)). The candidate selection criteria differs greatly from the SLACS. However, their similarities lie in that they both perform follow-up observations of the candidates, to determine which of them are lenses, although the SQLS uses a range of optical and infra-red telescopes and not the HST (Inada et al. 2008).

Figure 3.3, presents the candidate selection procedure of the SQLS (Inada et al. 2008) [§]. An initial statistical sample of quasars was selected from the SDSS spectroscopic QSO catalog (Schneider et al. 2005, 2007), using three parameters; redshift ($0.6 \leq z \leq 2.2$), i-band filter magnitude ($15.0 \leq i_{cor} \leq 19.1$) and maximum PSF (point spread function) width of $1.8''$ (Oguri et al. 2006). The first two criteria were selected as the low-redshift ($z \leq 2.2$) quasar target selection at $i_{cor} \leq 19.1$ is almost complete, while if the seeing is bad, the third criterion removes close lens pairs that can be mistaken for single PSF and vice versa (please see (Oguri et al. 2006) for more details). This method selected parent populations of 22,682 (Inada et al. 2008) and 36,287 (Inada et al. 2010) quasars respectively from DR3 and DR5. To obtain a sub-sample of lens candidates from the parent poulations, they implemented morphological and colour selection methods outlined by Pindor et al. (2003).

The morphological method selects candidates with multiple stellar components by fitting two PSFs and deriving the image separations, while the colour selection method selects sources with adjacent stellar components with similar colours (Oguri et al. 2006). Using this method they were able to reduce the parent populations to 220 lens candidates (Inada et al. 2008) from DR3, and 136 lens candidates (Inada et al. 2010) from DR5 for follow up observations. The follow up observations consisted of optical spectroscopy, optical imaging, and near-infrared imaging, conducted at the following facilities: the University of Hawaii 2.2 m telescope (UH88), the Astrophysical Research Consortium 3.5 m telescope (ARC 3.5 m), the Keck I and II telescopes, the United Kingdom Infra-Red Telescope (UKIRT), the Subaru telescope, the Magellan Consortium's Walter Baade 6.5 m telescope (WB 6.5 m), the HST, the MDM 2.4 m telescope (MDM 2.4 m), the MMT Observatory, the European Southern Observatory 3.6 m telescope (ESO 3.6 m), the New Technology Telescope (NTT), and the WIYN telescope. The

[§]A full description of this method is beyond the scope of this thesis, for a full description please see the given references for more details.

SQLS success rate for the DR3 survey was $\sim$ 5%, while the DR5 SQLS selection was at $\sim$ 26%.

3.3.2 The Cosmic Lens All-Sky Survey (CLASS) and the Jodrell Bank VLA Astromeric Survey (JVAS)

Prior to both SLACS and SQLS, CLASS/JVAS was the largest complete sample of strong lenses (Myers et al. 2003; Browne et al. 2003; Chae 2003). Both CLASS and JVAS are surveys of flat-spectrum radio sources designed to identify gravitational lens candidates, with suspected lenses followed up by higher resolution VLBA and MERLIN studies. Flat-spectrum radio sources were selected as they appear compact (point-like) to lower-resolution instruments such as the VLA. Lensing of compact sources is easier to recognise than lensing of extended sources. JVAS and its associated analysis was completed in 1992, leading to the discovery of 5 new gravitational lenses, and 1 rediscovery (Patnaik et al. 1992; King et al. 1999).

CLASS (an extension of JVAS) began in 1993, consisted of a complete sample of 13,783 flat-spectrum radio sources was observed with the VLA (Very Large Array) at 8.46 GHz in A configuration (resolution of $\sim$ 0.2 arcsec). Figure 3.4 illustrates the fundamentals of the CLASS search criteria, only a simple description of this method will be given here as a full description is beyond the scope of this thesis, for more information please see Myers et al. (2003); Browne et al. (2003); Chae (2003); McKean et al. (2007). This parent population was selected using the 1.4 GHz NVSS (National Radio Astronomy Observatory Very Large Array Sky Survey; Condon et al. (1998)) and the 4.85 GHz GB6 (Green Bank 6 cm; Gregory et al. (1996)) catalogues to find all flat-spectrum radio sources. The CLASS complete sample was selected by finding all sources with $S_{4.85} \geq$ 30 mJy from the GB6 catalogue within an area of sky $0^o \leq \delta \leq 75^o$ (Myers et al. 2003; Browne et al. 2003; McKean et al. 2007). These sources were then cross-correlated with the NVSS catalogue, and all sources with a spectral index, $\alpha_{1.4}^{4.85} \leq -0.5$ (where $S_\nu \propto \nu^\alpha$), were selected, for further observations with the VLA. From amongst these 13 000+ sources, hundreds of multiple-components were identified and followed up with higher resolution instruments such as the Multi-Element Radio Linked Interferometer Network (MERLIN; 50 mas resolution) and the Very Long Baseline Array (VLBA; 2 mas resolution) (Browne et al.

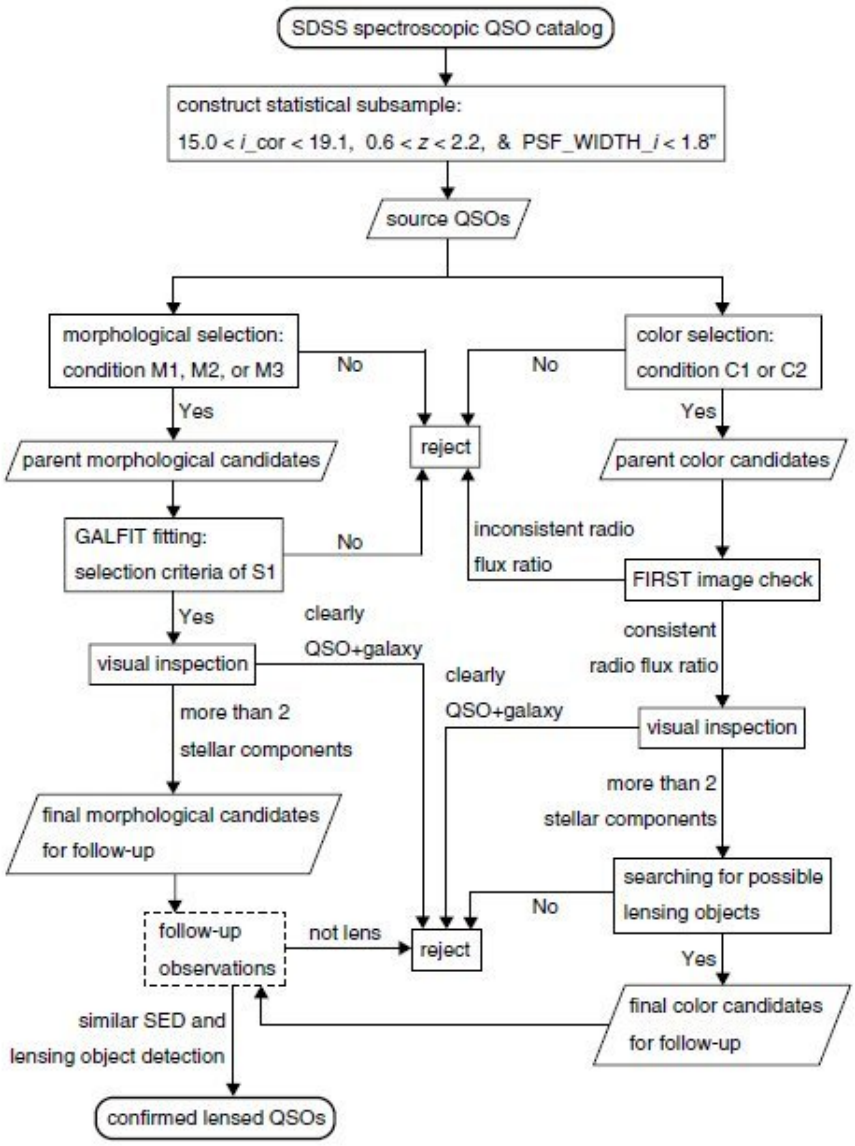

Figure 3.3: Flowchart of the candidate selection procedure of the SQLS Inada et al. (2008).

2003). From this CLASS has discovered 16 new radio-loud gravitational lens systems, which when added to the 6 JVAS lenses gives a total of 22 confirmed lens systems in the JVAS/CLASS gravitational lens survey (Myers et al. 2003). Figure 3.5, shows the 22 JVAS/CLASS lensed systems.

CLASS is the most complete gravitational lens survey to date (Browne et al. 2003). It has found gravitational lensed systems down to a separation of $0.3''$ and a maximum flux ratio of 10:1. Its completeness in parameter space is unlikely to be reached by any current optical survey.

3.4 Wide-Field Gravitational Lensed Surveys

3.4.1 COSMOS Lens Survey

Wide-field imaging presents an alternative to the traditional source/lens based gravitational lens surveys such as SLACS, SQLS and CLASS. This technique was first attempted in the Hubble Space Telescope Medium Deep Survey (Griffiths et al. 1994; Ratnatunga et al. 1999), the Great Observatories Origins Deep Survey field (GOODS;Fassnacht et al. (2004)), the AEGIS survey (Moustakas et al. 2007) and the SL2S (Cabanac et al. 2007). However these surveys were limited to finding systems with large deflection angles ($\theta_i > 3.0''$) because of seeing limitations (Faure et al. 2008). However, spaced based deep wide-field surveys such as the *HST* COSMOS survey (Scoville et al. 2007b) can easily resolve systems with smaller deflection angles (Faure et al. 2008). The *HST* COSMOS survey, provides an excellent opportunity to locate and study a large number of strong galaxy-galaxy lensing systems, as it includes the largest contiguous high-resolution astronomical imaging survey ever performed from space (Faure et al. 2008).

The *HST* COSMOS Lens Survey, is the first of such surveys to detect galaxy mass strong lens candidates Faure et al. (2008). They discovered 67 new massive early-type lens candidates with arcs found at radii smaller than $\sim 5''$. The total viewing angle of the *HST* COSMOS Lens Survey is 1.64 deg^2 and comprised observations from the *HST* ACS high-resolution imaging, the *Subaru* [¶] Suprime imaging, and the CFHT [‖] Megacam multicolor imaging.

[¶] www.naoj.org/

[‖] Canada-France-Hawaii Telescope: www.cfht.hawaii.edu/Science/CFHLS/

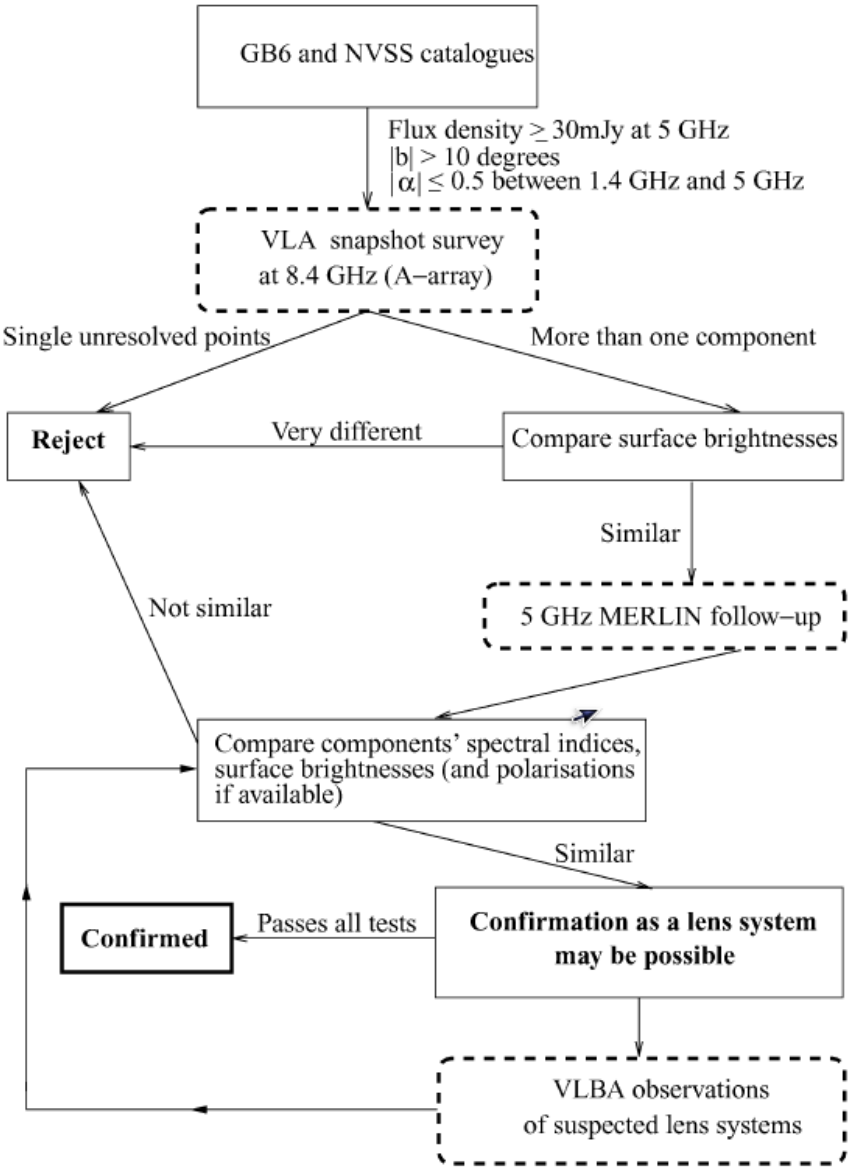

Figure 3.4: Flowchart of the candidate selection procedure of CLASS Browne et al. (2003).

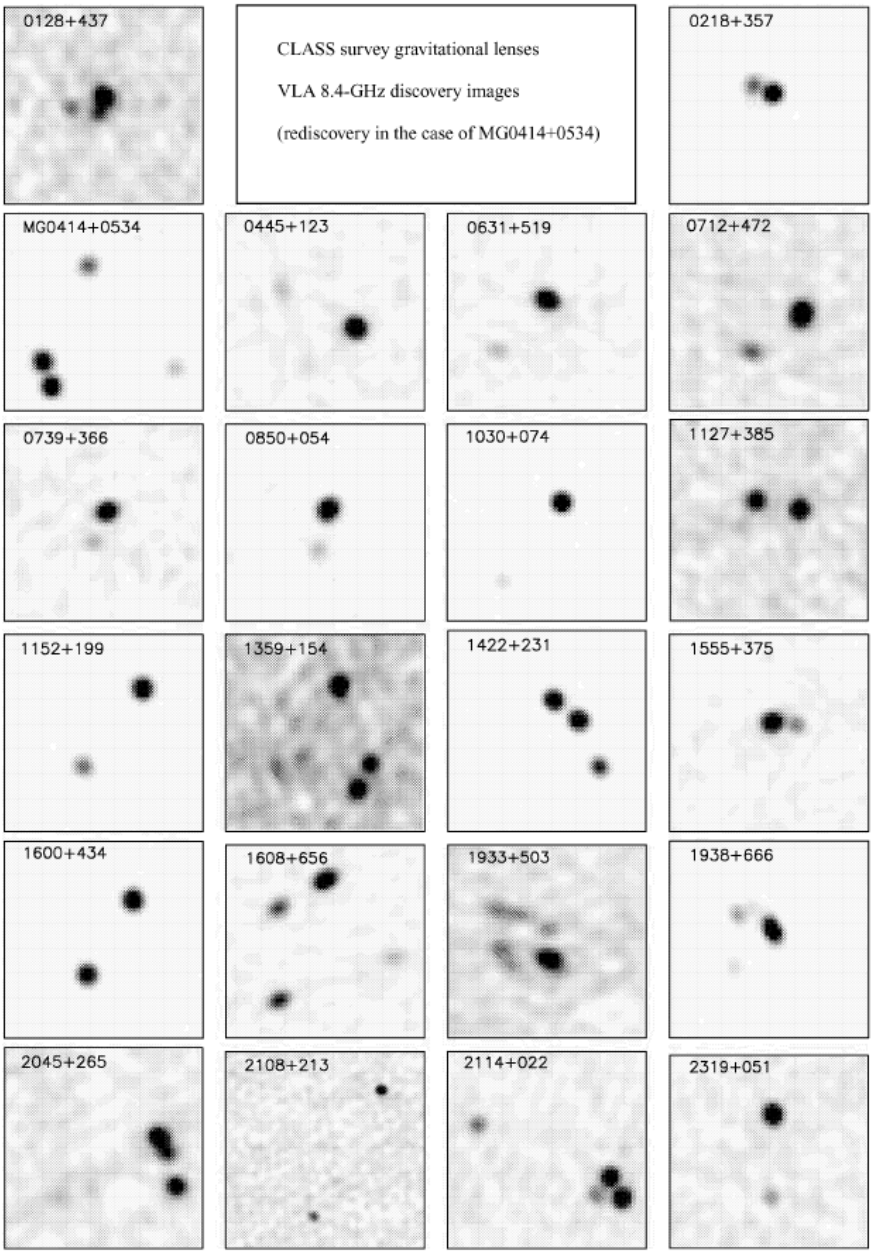

Figure 3.5: VLA 8.4 GHz discovery maps of the 22 successful radio-loud gravitational lenses from the CLASS survey Browne et al. (2003).

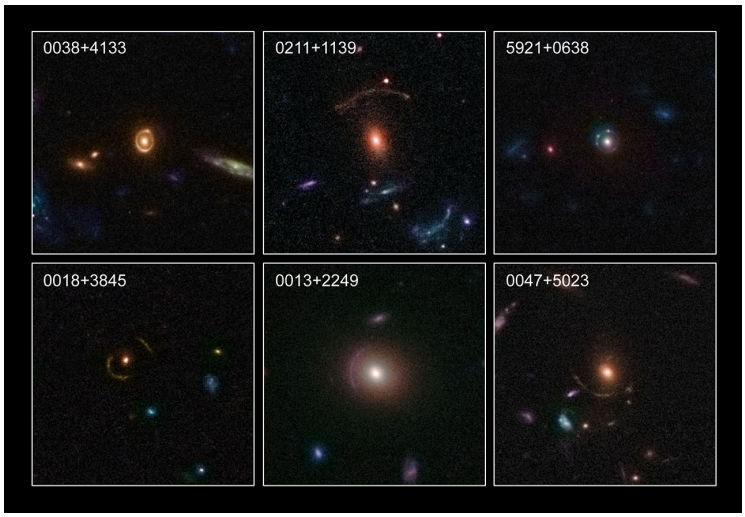

Figure 3.6: 6 of the 67 lens discovered by the COSMOS Lens Survey (Faure et al. 2008). *Image Credit:*NASA, ESA, C. Faure (Zentrum fr Astronomie, University of Heidelberg) and J.P. Kneib (Laboratoire d'Astrophysique de Marseille)

To identify the strong galaxy-galaxy lens candidates, they implemented a four step procedure which we will briefly describe (see Faure et al. (2008) for detailed descriptions of the following steps):

1. 9452 potential elliptical lenses were selected from the photometric red-shift catalogue (P catalogue).

2. Visual inspection of the ACS images of all galaxies in the P catalogue produced a catalogue of 337 potential strong galaxy-galaxy lens systems.

3. The E catalogue was investigated using multicolour images to check for color differences between the main galaxy and the potentially lensed object.

4. The foreground galaxy was then subtracted, by using a galaxy surface brightness model, to determine the morphology and lensing configuration of the potentially lensed background galaxy.

67 systems was able to pass these two final steps and qualify as strong galaxy-galaxy lens candidates, 20 of of these systems display multiple images or strongly curved large arcs. Finally, this study gives a lower limit of at least 10 strong lenses per square degree on the number of strong lenses expected in future deep space surveys. Figure 3.6, gives a sample of the 67 lens candidates discovered.

Chapter 4

Sample Selection and Simulations

4.1 Initial Source Population

The initial dataset for this survey (the "parent population") was taken from the sixth data release (DR6) of the United Kingdom Infrared Telescope (UKIRT) Infrared Deep Sky Survey (UKIDSS) The UKIDSS project is defined in Lawrence et al. (2007). UKIDSS uses the UKIRT Wide Field Camera (WFCAM; Casali et al. (2007)). The photometric system is described in Hewett et al. (2006), and the calibration is described in Hodgkin et al. (2009). The pipeline processing and science archive are described in Irwin et al (2010, in prep) and Hambly et al. (2008).

A total of 24,869 sources (in *YHK* wavebands) from the DR6, were inspected by eye for extensions, using a graphical user interface program, written in the C programming language. All sources with an extension or multiple stellar components, within a radius $\leq 3''$ from the source centre was selected as a *possible lens candidate*. The SQLS and CLASS found that all galaxy mass lenses were within a maximum separation of $3''$ (Inada et al. 2008; Browne et al. 2003). This eye inspection was done independently by two investigators (the author and Dr. Neal Jackson), and together identified 461 *possible lens candidates*. Of the 461 candidates, 28 were previously ruled out as gravitational lenses (by SQLS), and included 9 previously discovered lensed systems: SDSS J0806+2006 (Inada et al. 2006); SDSS J0820+0812 (ULAS J0820+0812) (Jackson et al. 2009); SDSS J0832+0404 Oguri et al. (2008); RX J0911+0551 (Bade et al. 1997); SDSS J0924+0219 (Inada et al. 2003); SDSS J1226-0006 Inada et al. (2008); SDSS J1322+1052 Oguri et al. (2008); SDSS J1353+1138 (Inada et al. 2006); SDSS

J2343-0050 (ULAS J2343-0050) (Jackson et al. 2009).

The *possible lens candidates*, were then selected for a second process to determine the *most probable lens candidates*. For each of the 461 candidates, SDSS *ugriz* data were obtained from the SDSS quasar catalogue (DR6, Adelman-McCarthy et al. (2008a)).

4.2 Selection Algorithm

In this section we will discuss the second selection criteria, based upon the morphological and colour trend reported by Jackson et al. (2009). Recall (Section 1.2) Jackson et al. (2009), discovered that the image separation, $\Delta\theta_i$ between both lensed images (A & B) of the gravitational lens ULAS J2343-0050 decreased with increasing wavelengths (i.e. from ultra-violet to infra-red wavelengths). To observe this effect they used a combination of SDSS *ugriz* and UKIDSS *JHK* observations of ULAS J2343-0050. Thus the main assumption of this selection criteria, is that **all candidates that show a decrease in separation between the two main images (A & B) with increasing wavelength**, will be selected in the final sample, as *most probable lens candidates* for further observations with the Keck telescope.

To select the *most probable lens candidates* from the 461 *possible lens candidates*, we developed a semi-automated method written entirely in the Python Programming Language *. The semi-automated method is broken into 4 parts, each serving a different function:

1. The initial SDSS *ugriz*, data for the 461 candidates are wide-field scans of approximately $820'' \times 700''$, with our candidates located within these large scans. The first part of our semi-automated method, simply locates and cuts out the candidates into a smaller 32×32 pix squared image. Note this is done only for the SDSS images.

2. To measure the image separations, the main part of the algorithm fits two gaussians to A and B, which required that the positions of A & B be estimated. During the early tests the determination of the positions were tried automatically. However, most of the observations suffered from contamination from bright background or nearby stellar objects, which sometimes

*www.python.org/

were mistaken for image B. To solve this problem, the image positions were determined by eye using a Python graphical program. During the SDSS observations the bands *ugriz* were observed simultaneously, and hence have the same properties (i.e size, orientation, position etc). Thus the location of an object would most likely remain relatively constant across all bands. This allows the positions obtained for a source in one SDSS band to be used to constrain the position for all SDSS bands. This assumption also holds true for the UKIDSS *YHK* bands.

3. After the positions of A and B were determined, the separation, $\Delta\theta_i$ between them were calculated by fitting the two gaussians to the positions of both components. This fitting was done with the task JMFIT from the National Radio Astronomical Observatory (NRAO) data package AIPS. This task was implemented within the Python script using the ParselTongue [†] scripting language written in Python for AIPS. A FWHM (full-width at half-maximum) of 2 pixels, was used for the fitting gaussians. This was found to be the optimal value, since larger FWHMs caused significant overlapping at $\Delta\theta_i < 1.4''$. The separation, $\Delta\theta_i$ was calculated

$$\Delta\theta_i = \sqrt{(x_1 - x_2)^2 + (y_1 - y_2)^2} * P \tag{4.1}$$

where (x_1,y_1) and (x_2,y_2) are the maxima positions of both components from the gaussian fitting, and P, is the pixel to arcsecond conversion which is 0.396 for the SDSS (York et al. 2000a) and 0.403 for the UKIDSS (Lawrence et al. 2007) respectively. Similarly, the separation error, σ_s,

$$\sigma_{\Delta\theta_i} = \sqrt{(\frac{x_1 - x_2}{(\Delta\theta_i/P)})^2 * (\delta_{x_1}^2 - \delta_{x_2}^2) + (\frac{y_1 - y_2}{(\Delta\theta_i/P)})^2 * (\delta_{y_1}^2 - \delta_{y_2}^2)} * P \tag{4.2}$$

where $(\delta_{x_1}, \delta_{y_1})$ and $(\delta_{x_2}, \delta_{y_2})$ are the positional errors of A and B obtained from JMFIT.

4. The final part of the algorithm, looks for a general decrease of $\Delta\theta_i$ with

[†]www.jive.nl/dokuwiki/doku.php?id=parseltongue:parseltongue

increasing wavelength. The algorithm fits a weighted linear regression between $\Delta\theta_i$ against wavelength, using the generalized least-squares regression(GLR) model from the scikits.statsmodels.regression [‡] module from the Scientific Python (scipy)[§]. The GLR was preferred as it allows a very flexible and straightforward use of weighting. A standard weighting $(1/\sigma^2_{\Delta\theta_i})$ for each wavelength per source was implemented, . Sources that were found to have a gradient $\leq$ -0.05 were selected as *most probable lens candidates*, while those with a gradient -0.05 were rejected.

4.3 Lens Simulation

To quantify the completeness (i.e number of false negatives) of our 4-step selection procedure, simulations were performed aimed at "mimicking" the typical lenses expected to be discovered with the above selection criteria. Such lenses are basically 2-component lensed systems, with a red elliptical lens galaxy. The simulation implemented both morphological and colour properties typical of such lenses.

Firstly, a 2-dimensional grid of size 32 $\times$ 32 square pixels was generated. The pixel to arcsecond scale was taken to be 0.4, which is approximately the size of the UKIDSS and SDSS pixel to arcsecond scales. To simulate the typical double lensed images, two simple gaussian type PSFs (Point Spread Function) was then added along with some background noise to the grid, implemented with a python gaussian algorithm. The PSFs of the UKIDSS and SDSS are $0.8''$ (Lawrence et al. 2007) and $1.4''$ (York et al. 2000a). This corresponds, in our grid to a PSF FWHM of 3.0 and 2.0 pixels for the *ugriz* and *YHK* wavelengths, respectively.

A typical elliptical galaxy model was placed between the two gaussians, but in a position closer to the fainter image. The galaxy model was obtained from images of the COSMOS galaxy survey (Scoville et al. 2007a). As discussed previously (Section 1.2), the decrease of the image separation with increasing wavelength, is due to the flux of the galaxy near the fainter image (B), increasing with wavelength. To simulate this colour dependence of a typical red elliptical galaxy, we used the ultraviolet to near-infrared spectra template for an elliptical galaxy given by Kinney et al. (1996), redshifted to z = 0.5 (figure 4.1). For the purpose of this

[‡]http://statsmodels.sourceforge.net/regression.html
[§]www.scipy.org

simulation, we are only interested in a first order approximation to the effect of wavelength on the flux of the galaxy. The data set used in this study spans an order of magnitude in wavelength from ultraviolet to infrared (3600 Å - 22000Å). The template shown in figure 4.1, is fitted with a simple linear regression model in 3 regions: a.3000-4000 Å; b.4500-8000 Å; c.8000-12000 Å. The plateau from 8000-12000 Å, generally continues well into the infrared wavelengths (Kinney et al. 1996), thus will apply to the H (16300 $Å^{-1}$) and K (22000 Å) bands. The 3 linear regression models are:

$$F_\lambda = -3.4929 \times 10^{-8} \times \lambda + 3.3405 \times 10^{-4};\ for\, u\, band \tag{4.3}$$

$$F_\lambda = 1.54738 \times 10^{-6} \times \lambda - 6.8085 \times 10^{-3};\ for\, gri\, bands \tag{4.4}$$

$$F_\lambda = 9.05332 \times 10^{-8} \times \lambda + 4.5754 \times 10^{-3};\ for\, zYHK\, bands \tag{4.5}$$

The above equations are scaled to 10^{-14} and the flux unit is $10^{-14}\, ergs\, s^{-1} cm^{-2}\, Å^{-1}$, and Å for the wavelength. However for the simulation, we are interested in only the relative values and variation with wavelength and not the absolute values.

A colour dependence of the "background quasar" was also introduced into the algorithm in the form of a simple power law; $S_Q \propto \nu^\alpha$, where S_Q is the brightness of the lensed quasar images (A and B), ν is the wavelength, and α is the spectral index of quasar. For this simulation a typical α of -0.5 is assumed (Gregg et al. 1996). Hence, as the wavelength increases, the brightness ratio tends to favour the red galaxy, moving the peak of the PSF towards A. Thus giving the impression that the separation between A and B is decreasing.

Another important criteria considered in the simulations is the brightness ratio, F_r between A and B. The CLASS survey, found that the maximum detectable flux ratio between the two images was 10:1 (Myers et al. 2003; Browne et al. 2003). Also, Jackson et al. (2009), assumed that this technique will be able to detect lenses with a maximum flux ratio of 10:1. To test the limits and completeness of this survey, we adopted a flux ratio of 15:1 for the simulation. For each simulated lens this value was randomly selected.

An initial image separation range of $1.0'' < \Delta\theta_i < 3.0''$ was introduced at the start of each simulation. Although, Jackson et al. (2009), suggested that the minimum $\Delta\theta_i$, detectable by this technique was $0.6''$, it was very difficult

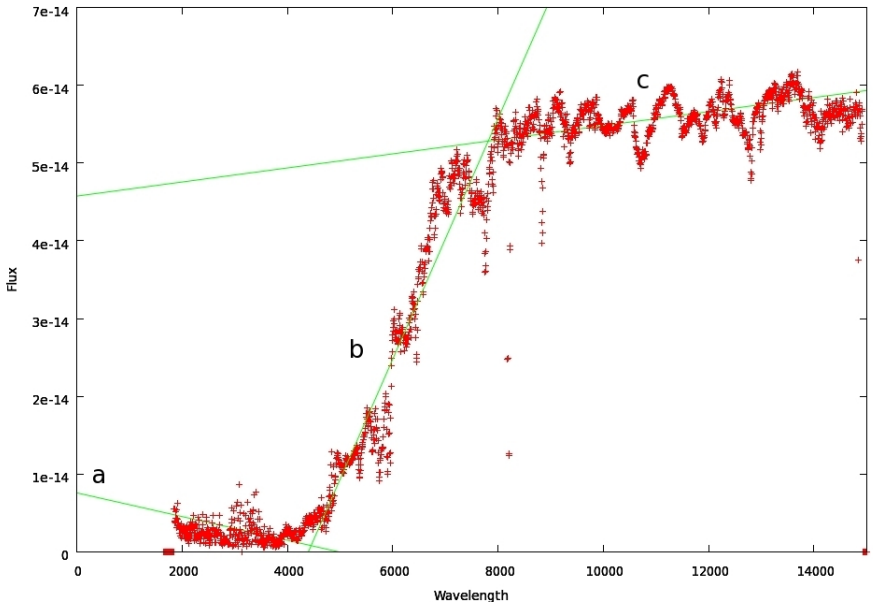

Figure 4.1: Ultraviolet to near-infrared spectra template for an elliptical galaxy from Kinney et al. (1996). The lines shows the model fitting for the 3 regions described by equations 4.3,4.4 and 4.5. The units are $10^{-14}\, ergs\, s^{-1} cm^{-2}\, \text{Å}^{-1}$ for the flux and Å for wavelength.

to successfully fit the 2 gaussians to determine the positions of A and B for systems with $\Delta\theta_i < 1.''0$. Both CLASS and SQLS indicated that the maximum separation for galaxy-mass lens is $3.0''$ (Myers et al. 2003; Inada et al. 2008). This value was also randomly selected at the start of each lens simulation.

49 lensed systems were simulated based upon the above descriptions. All simulated lenses under a flux ratio of 6:1 ($\sim$ 30 sources), were successfully selected by the 4-step procedure. However, only 6 simulated lenses above a flux ratio of 6:1 were selected, while the remaining 13 were rejected. For simplicity, the position of A was kept constant. Table 4.1, presents the properties of the 49 simulated lenses (including the 13 false negatives), such as brightness ratio between A and B (F_r), initial image separation ($\Delta\theta_i$) and the gradients obtained from the GLR model.

The simulations indicate that this survey is 100% complete for lenses within image separation range of $1.0'' < \Delta\theta_i < 3.0''$ and flux ratio, $F_r \leq 6$. However for $F_r > 6$ we have a $\sim$ 46% probability of identifying the object as a lens system.

Table 4.1: Properties of the 49 simulated lens. *Column 1* gives the simulation number; *Column 2* gives the flux ratio, F_r between A and B used at the start of the simulation; *Column 3* gives the initial separation of the images and *Column 4* gives the gradient of the GLR model. The last 13 rows give the rejected lenses.

Simulation Number	Flux Ratio F_r	Initial Image Separation $\Delta\theta_i$ (arcseconds)	m
1	2.31	2.16	-0.18
2	2.74	2.01	-0.50
3	5.58	2.92	-0.22
4	3.94	1.67	-1.55
5	2.40	1.75	-0.34
6	2.40	1.86	-0.42
7	3.24	3.00	-0.23
8	2.70	2.64	-0.22
9	2.06	2.88	-0.16
10	4.56	2.75	-0.16
11	5.27	2.22	-0.82
12	1.06	2.19	-0.26
13	3.62	2.37	-0.30
14	2.51	2.43	-0.85
15	4.18	1.98	-1.36
16	1.29	1.02	-0.07
17	5.35	1.82	-1.67
18	2.84	2.65	-0.22
19	1.98	2.90	-0.09
20	3.88	2.80	-0.32
21	4.78	2.91	-0.10
22	1.68	2.20	-0.49
23	4.47	1.54	-0.33
24	3.66	1.03	-1.22
25	1.71	1.63	-0.15
26	4.65	1.09	-0.92
27	1.84	1.44	-0.13
28	2.50	1.47	-1.23
29	4.18	1.64	-1.50
30	1.61	1.71	-0.37
31	14.40	2.62	-0.34
32	9.15	2.49	-0.06
36	12.21	2.55	-0.05
37	12.16	2.73	-0.06
39	10.80	2.58	-0.06
44	13.83	2.64	-0.05
46	13.28	2.77	-0.05
33	9.63	1.29	0.17
34	8.51	1.03	0.01
35	9.10	1.49	0.25
38	14.52	2.29	0.16
40	7.61	1.13	0.23
41	14.25	2.29	0.22
42	11.54	1.83	0.00
43	6.55	1.89	-0.04
45	11.07	2.07	0.02
47	13.89	2.38	0.23
48	15.00	2.04	0.08
49	9.09	1.36	0.12

Chapter 5

Results

Using the 4-step procedure described in section 4.2, 132 sources showed a general decrease in image separation with increasing wavelength. 8 out of the 9 known gravitational lensed systems (See Chapter 4.1) were successfully recovered in the P catalogue, suggesting that this method has an $\sim$ 89 % success rate in detecting lenses. The remaining lensed system, 132236.4+105239 increased in image separation in the *YH* infrared bands, which could be due to a sudden decrease in the flux of the galaxy at these wavelengths. Figure 4.1 shows a sudden decrease at $\sim$ 8000 A, for a lens galaxy at redshift, z = 0.5. At a corresponding redshift this may coincide at the *YH* bands. This was not accounted for in our survey and simulation, which led to the rejection of 132236.4+105239. Additionally, 10 of the 28 previously rejected lens candidates, displayed an apparent decrease in image separation with wavelength and are hence selected as *most probable lens candidates*.

The remaining 113 sources, have been further sub-divided into 3 sub-catalogues; the A list, B list and the C list of lens candidates. The division is based upon the *weighted average image separation*, $\Delta\theta_w$ over all wavelengths. $\Delta\theta_w$, was used as opposed to the maximum image separation, or the image separation at the shortest wavelengths, because of the large variation of $\Delta\theta_i$ for some sources. It is believed that $\Delta\theta_w$, will give the most reliable, estimation of the overall $\Delta\theta_i$. This sub-division is necessary as there are some sources with $\Delta\theta_w$, lying outside the optimal detection range of $1.0'' < \Delta\theta_i < 3.0''$ of this survey obtained from the simulations (see Chapter 4.3).

Sources within the range, $0.8'' < \Delta\theta_i < 3.0''$ (note, $0.8''$ is the PSF width of UKIDSS, see Sections 1.2 and 4.2) are selected in the A list, while sources

above 3.0″ are in the B list and those less than 0.8″, are relegated to the C list. It was noted earlier that the limiting separation for this survey is 0.8″, which is the resolution of the UKIDSS PSF. Therefore, one can expect that any potential lensed system with a $\Delta\theta_i < 0.8''$, to have a very high uncertainty in its credibility. Therefore, we will reject the C list sources (which contains 22 sources), although they display the expected decreasing image separation for gravitational lens. Additionally, the $\Delta\theta_i$ of the C list sources show a much larger dispersion with wavelength, compared to the A and B list.

We do not reject the B list source, since they show multiple components that fall within the 3.0″ radius. The 87 A list sources and the 3 B list sources are listed in table 5.1, including the gradient, flux ratio, weighted image separation, and the image separation for each wavelength. Although not included in the sub-catalogues, all 8 known gravitational lenses and 6 known rejects fall within the A list, which suggests that our survey has a $\sim$ 21% false positive rate (i.e. $\sim$ 79% reliability). Figures 5.1 - 5.7 shows either the *Y, H or K* band images of the final list of 90 sources (hereafter, the P catalogue).

Table 5.1: The **A and B list** of potential gravitational lensed sources. The 3 B list sources are listed at the end.

Source[a]	m[b]	F_r[c]	$\Delta\theta_w$[d]	$\Delta\theta_u$[e]	$\Delta\theta_g$	$\Delta\theta_r$	$\Delta\theta_i$	$\Delta\theta_z$	$\Delta\theta_Y$	$\Delta\theta_H$	$\Delta\theta_K$
000440-000146	-0.56	12.31	1.16	-99	1.62	0.76	0.74	1.35	-99	1.07	1.29
000508+010806	-0.25	3.47	1.61	2.01	1.60	1.54	1.46	1.72	1.43	1.76	1.23
000508+002608	-0.82	1.00	2.36	2.47	2.42	2.40	2.41	-99	2.32	2.39	1.13
000602-005358	-2.04	4.96	0.84	-99	2.31	0.44	-99	1.89	0.63	1.56	1.66
003901-003544	-0.38	4.70	1.12	1.58	1.25	1.12	1.91	1.93	1.76	1.49	1.27
004116+000013	-0.86	4.74	2.37	1.30	1.79	2.37	1.90	-99	1.33	0.44	2.04
004452-000826	-0.83	1.35	1.47	-99	1.41	-99	1.10	1.47	2.55	2.22	2.34
010456+151557	-0.21	7.75	1.57	-99	-99	2.04	2.05	2.05	1.57	1.64	1.76
010507+002441	-0.28	4.03	2.57	1.95	2.53	2.67	2.50	-99	2.57	2.03	2.41
010605-005951	-0.10	7.73	2.05	-99	2.00	2.69	1.91	1.69	1.65	1.69	1.56
012559+001829	-0.25	1.88	2.11	2.10	2.08	2.13	2.26	2.90	-99	2.06	2.28
013439+001732	-0.39	7.69	2.69	-99	2.99	3.03	2.57	3.01	3.06	2.86	2.22
014349+002128	-0.82	1.32	1.69	2.77	1.68	1.74	1.71	1.66	0.27	1.51	1.48
020547-010702	-1.32	17.52	2.46	-99	3.13	2.20	2.52	2.40	2.46	2.40	2.50
022045+011253	-0.09	6.71	2.44	-99	2.10	2.44	2.44	1.65	2.31	2.59	2.34

Continued on Next Page...

Table 5.1 – Continued

Source	m	F_r	$\Delta\theta_w$	$\Delta\theta_u$	$\Delta\theta_g$	$\Delta\theta_r$	$\Delta\theta_i$	$\Delta\theta_z$	$\Delta\theta_Y$	$\Delta\theta_H$	$\Delta\theta_K$
023913-005122	-0.89	13.48	1.32	-99	1.71	0.18	1.37	1.60	-99	0.95	1.31
024308-000127	-0.46	4.75	1.91	-99	2.11	1.91	2.18	2.17	2.03	1.19	1.99
025314-003903	-0.13	3.26	2.89	3.15	1.39	3.11	2.92	3.08	2.92	3.04	2.91
025432-004933	-0.41	10.90	2.16	2.40	2.80	2.05	1.96	1.91	2.12	2.15	1.99
031005-011231	-0.08	10.38	2.76	2.56	3.12	3.89	3.33	3.11	3.07	3.05	2.99
031538+010422	-0.61	17.91	0.98	-99	0.98	0.70	0.55	0.21	2.07	0.94	0.02
031652-000658	-0.52	6.94	2.24	-99	1.97	2.20	2.17	2.92	2.51	2.28	1.95
032506-010028	-0.14	4.50	2.10	-99	2.17	2.23	2.04	2.21	2.07	2.02	1.92
034408-003106	-0.06	1.90	2.91	3.04	3.07	3.01	3.02	2.91	-99	3.02	2.92
075056+214150	-0.46	3.43	1.27	1.71	1.91	0.19	0.37	1.49	1.87	1.66	1.70
080142+223416	-0.25	7.57	2.42	2.76	1.33	2.41	2.57	2.42	2.45	2.58	2.45
080705+221039	-0.9	9.32	2.77	2.73	2.60	2.73	2.73	2.77	2.79	2.73	2.76
081909+031904	-0.32	1.14	1.81	1.84	1.76	1.74	1.74	1.71	-99	1.23	2.41
081910+211740	-0.14	12.20	1.90	2.99	1.79	1.71	1.61	1.73	1.71	1.76	1.61
083609+065914	-7.23	21.45	2.72	3.60	0.65	2.79	2.69	2.72	2.69	2.70	-99
083655+075712	-0.25	8.87	1.82	1.69	0.30	0.24	1.69	1.83	1.79	1.79	1.79
085428+090733	-0.14	4.50	2.79	-99	-99	2.90	2.83	2.79	2.85	2.68	2.73
085850+045528	-0.4	1.37	1.90	2.16	1.89	1.92	1.89	1.72	-99	2.08	1.41
085939+010104	-1.21	14.45	1.80	2.53	1.11	1.79	2.55	1.56	2.33	2.50	2.31
090240+031151	-0.14	13.10	2.64	-99	2.82	2.71	2.55	2.59	-99	2.69	2.59
090535-004040	-0.57	7.22	1.81	2.51	1.85	1.79	1.80	1.80	-99	1.81	1.84
091329+043804	-0.47	3.24	2.20	2.37	-99	2.00	2.15	2.20	-99	2.12	2.22
092158+034236	-0.06	1.88	1.57	1.59	1.54	1.51	1.50	1.57	-99	1.42	1.50
093159+033622	-0.43	5.88	0.81	0.99	0.86	0.47	0.58	0.79	-99	1.51	0.49
093524+112017	-0.21	2.86	1.40	1.20	0.43	0.39	1.57	0.47	1.57	1.67	1.66
093750+020827	-1.07	13.01	2.92	-99	1.21	2.12	0.75	2.25	2.35	3.43	2.30
094933+062201	-0.3	11.59	2.10	-99	2.08	2.08	2.12	2.11	2.10	1.52	1.58
102836-004314	-0.5	12.59	1.98	3.15	0.73	0.82	2.2	2.35	2.26	0.6	0.54
102904+040309	-1.25	18.51	0.96	1.64	1.83	0.25	0.26	0.62	0.96	1.95	0.53
104837-002814	-0.06	4.06	2.58	2.53	2.63	2.63	2.63	2.58	-99	2.43	2.43
104959+025519	-0.72	12.57	1.87	1.60	1.83	-99	1.06	1.87	-99	2.00	0.84
105156+005018	-0.22	2.53	1.35	1.74	0.48	1.50	1.49	1.05	-99	1.35	1.24

Continued on Next Page...

Table 5.1 – Continued

Source	m	F_r	$\Delta\theta_w$	$\Delta\theta_u$	$\Delta\theta_g$	$\Delta\theta_r$	$\Delta\theta_i$	$\Delta\theta_z$	$\Delta\theta_Y$	$\Delta\theta_H$	$\Delta\theta_K$
105428+014343	-0.37	19.58	2.16	2.39	1.75	1.46	1.75	1.89	-99	1.91	2.62
111525+013407	-0.09	11.36	1.76	2.23	2.47	0.05	0.74	2.30	3.03	1.99	2.07
111817+074558	-0.18	7.42	1.63	1.66	1.73	1.60	1.56	1.70	-99	1.45	1.48
112646+074608	-0.59	7.40	0.89	-99	1.9	1.04	0.89	1.93	-99	2.13	2.03
113613+033841	-0.09	1.29	1.65	1.65	1.65	1.66	1.67	-99	1.66	1.59	1.49
115800+120439	-0.02	5.16	1.36	-99	-99	1.87	1.75	1.36	-99	1.74	1.71
120320+053137	-1.15	9.59	0.90	0.62	2.36	0.11	0.27	2.06	1.07	0.67	0.51
120359+095419	-0.43	2.58	1.48	1.92	-99	1.86	1.76	1.75	1.37	1.56	1.08
120749+082407	-0.29	0.87	0.97	1.74	1.35	1.38	1.06	1.32	0.20	1.29	1.38
121405+010205	-0.85	4.71	2.20	-99	2.18	2.17	2.16	1.58	2.13	2.29	2.21
122512+095420	-0.45	3.98	1.00	0.70	0.08	0.13	0.71	0.45	1.02	1.76	0.21
122726-001004	-0.06	7.14	2.54	2.77	2.49	2.53	2.58	2.59	-99	2.64	-99
123401+063215	-0.54	7.06	2.97	2.56	3.11	2.90	2.91	2.84	2.97	2.96	2.97
123526+150807	-3.78	5.87	1.49	-99	2.62	-99	2.91	3.01	2.97	3.00	2.99
131625+114601	-0.57	4.87	2.64	3.52	2.65	2.64	2.64	2.65	2.62	2.63	2.62
133245+115238	-0.94	4.95	1.05	1.59	0.08	0.17	2.71	2.48	2.39	2.70	1.27
140939+074842	-1.89	0.51	2.90	-99	2.94	2.91	2.89	2.90	2.84	2.76	1.19
141637+003352	-2.34	5.06	1.02	1.74	0.25	0.29	0.15	0.15	1.02	1.73	2.46
141954+072255	-0.66	4.70	1.02	1.42	0.12	1.72	1.73	1.15	1.01	0.77	0.74
142526-004422	-1.52	12.39	1.15	2.19	1.58	1.48	0.47	0.99	1.15	1.19	1.13
142808+044826	-0.92	4.57	1.66	2.66	-99	1.93	1.87	1.66	0.77	1.85	0.99
142917+012059	-0.37	6.76	1.82	2.01	1.83	1.61	1.79	1.84	1.92	1.79	1.28
143058+003505	-0.40	6.15	1.60	1.81	0.12	2.04	1.72	1.54	2.35	0.84	1.15
143117+103939	-0.27	6.15	2.11	-99	-99	2.11	2.21	2.66	2.16	2.12	2.09
151505+041012	-0.06	2.15	1.49	0.17	0.26	0.24	0.51	0.68	1.49	1.48	1.58
155446+093845	-0.14	0.61	2.13	2.98	2.03	-99	2.65	2.50	2.64	2.75	2.60
214041-004359	-1.09	2.07	2.05	2.08	2.03	2.06	2.07	2.06	1.88	0.48	2.05
214958+001128	-1.65	3.53	2.08	-99	2.08	2.20	2.17	2.17	2.18	0.33	2.29
215324+011437	-0.06	0.54	1.03	-99	1.14	1.18	0.84	1.08	1.18	1.15	1.05
215744+005304	-0.13	4.64	1.90	2.03	-99	1.93	1.82	1.18	1.22	2.84	0.71
220906+004544	-0.11	1.68	1.62	1.58	1.64	1.63	1.67	1.66	1.63	1.65	1.33
221926-004613	-0.09	3.30	1.94	-99	-99	1.98	1.94	1.85	1.82	-99	1.79

Continued on Next Page...

Table 5.1 – Continued

Source	m	F_r	$\Delta\theta_w$	$\Delta\theta_u$	$\Delta\theta_g$	$\Delta\theta_r$	$\Delta\theta_i$	$\Delta\theta_z$	$\Delta\theta_Y$	$\Delta\theta_H$	$\Delta\theta_K$
222417+011124	-0.26	2.16	1.37	1.69	0.2	1.46	1.16	0.97	-99	-99	2.71
2229295+010438	-0.05	1.02	2.20	-99	0.65	1.36	1.36	0.9	2.20	1.48	0.87
2251478+001641	-0.06	5.37	1.78	-99	1.8	1.87	1.78	2.14	1.89	1.72	1.85
231148+004426	-0.07	3.01	1.89	2.01	1.87	1.93	1.87	1.84	1.79	1.84	1.94
232221+010733	-1.29	2.11	1.03	1.92	0.26	-99	0.94	2.04	0.85	-99	1.83
233635-010734	-0.21	2.94	1.74	2.04	1.76	1.69	1.72	1.66	1.69	1.71	1.70
234623+010918	-1.29	0.99	1.85	-99	1.85	1.91	1.15	2.01	1.56	0.75	1.05
235344+005217	-0.64	9.37	2.48	-99	2.38	2.20	2.48	1.70	2.18	1.60	2.26
092659+062327	-0.62	4.15	4.05	4.41	4.44	4.23	4.05	3.99	-99	3.62	3.24
094122+051822	-1.81	4.83	3.73	5.37	4.97	4.18	4.04	3.93	-99	3.42	3.78
235643+001428	-0.18	10.32	3.46	3.73	2.52	3.41	3.41	3.50	3.10	3.28	3.02

[a]Source name in IAU J2000 format

[b]Gradient of image separation against wavelength

[c]Flux ratio in g band of both images

[d]Image separation weighted average

[e]Columns 5-12 gives the image separation in the *ugrizYHK bands* respectively. A value of -99 is given where either the data is missing or gaussian fitting was impossible due to bad data.

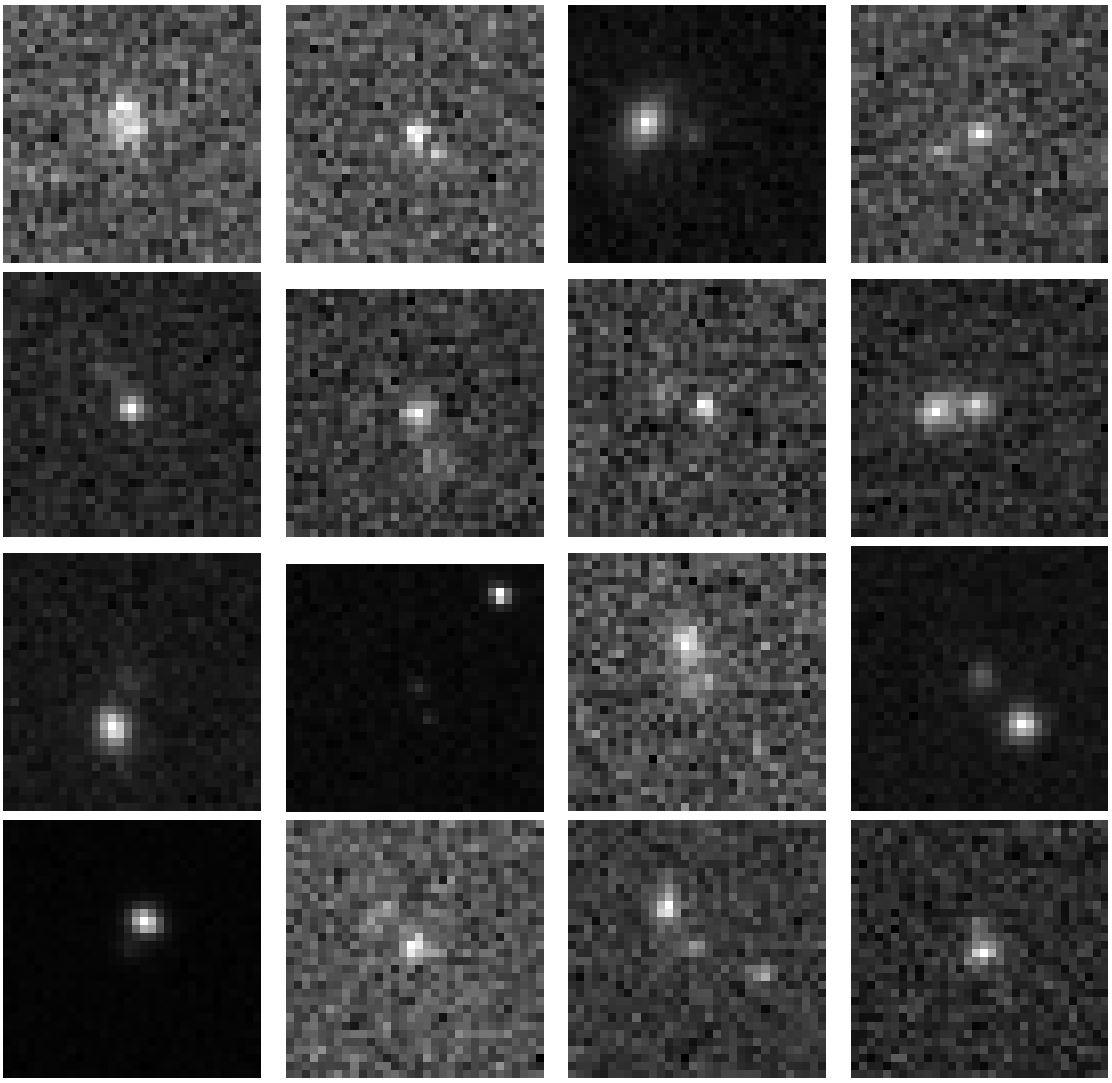

Figure 5.1: Sources from the A catalogue from left are, *first row*: 000440.0-000146, 000508.4+010806, 000508.9+002608, 000602.2-005358; *second row*: 003901.5-003544, 004116.0+000013, 004452.8-000826, 010456.6+151557; *third row*: 010507.3+002441, 010605.4-005951, 012559.2+001829, 013439.3+001732; *fourth row*: 014349.2+002128, 020547.3-010702, 022045.3+011253, 023913.6-005122

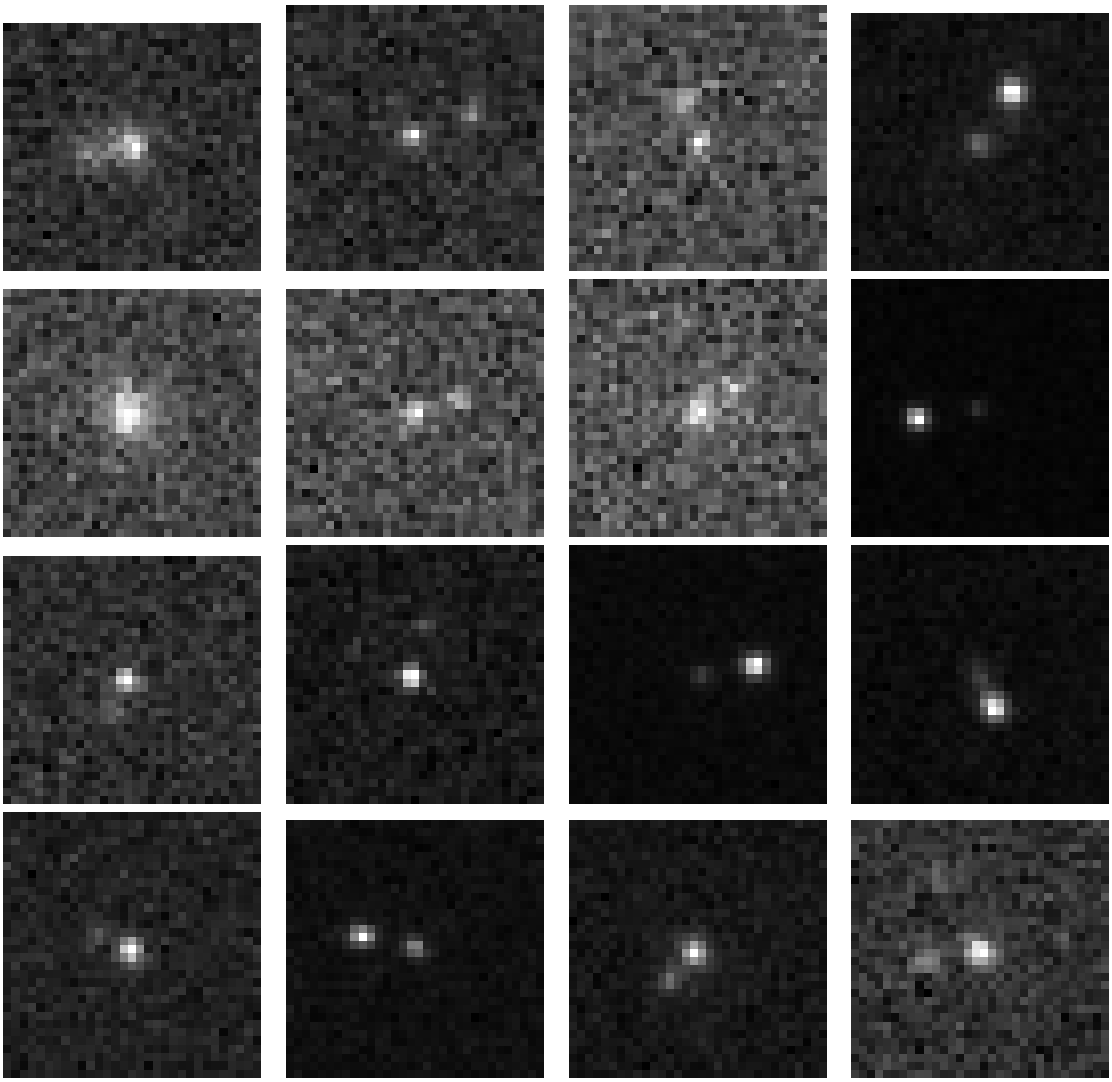

Figure 5.2: Sources from the A catalogue (continued) from left are, *first row*: 024308.2-000127, 025314.0-003903, 025432.3-004933,031005.2-011231 ; *second row*: 031538.7+010422, 031652.8-000658, 032506.9-010028, 034408.3-003106; *third row*: 075056.8+214150, 080142.6+223416, 080705.3+221039, 081909.9+031904; *fourth row*: 081910.2+211740, 083609.7+065914, 083655.0+075712, 085428.6+090733

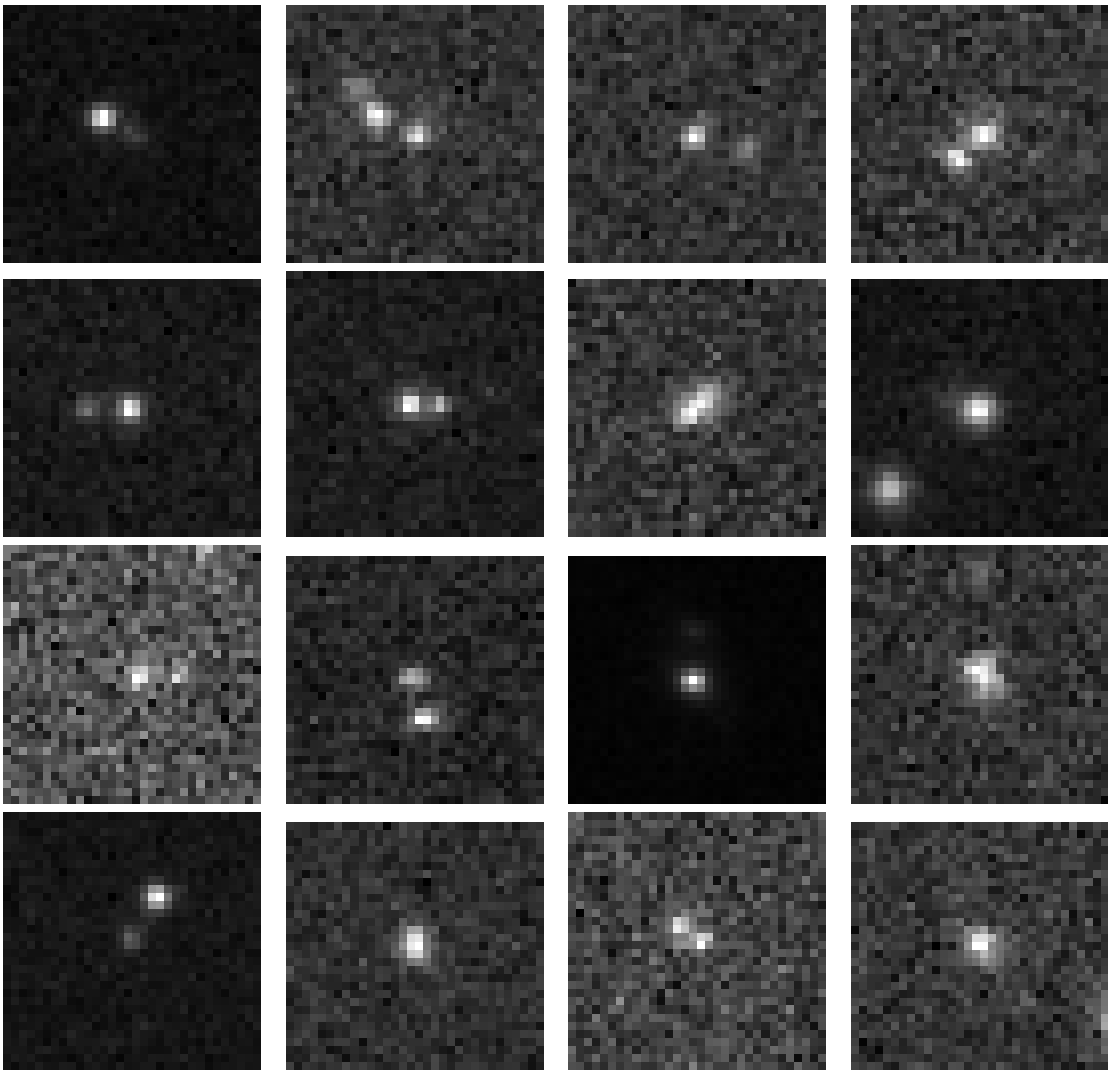

Figure 5.3: Sources from the A catalogue (continued) from left are, *first row*: 085850.2+045528, 085939.7+010104, 090240.2+031151, 090535.8-004040; *second row*: 091329.7+043804, 092158.9+034236, 093159.4+033622, 093524.7+112017; *third row*: 093750.1+020827, 094933.0+062201, 102836.9-004314, 102904.2+040309; *fourth row*: 104837.4-002814, 104959.7+025519, 105156.1+005018, 105428.3+014343

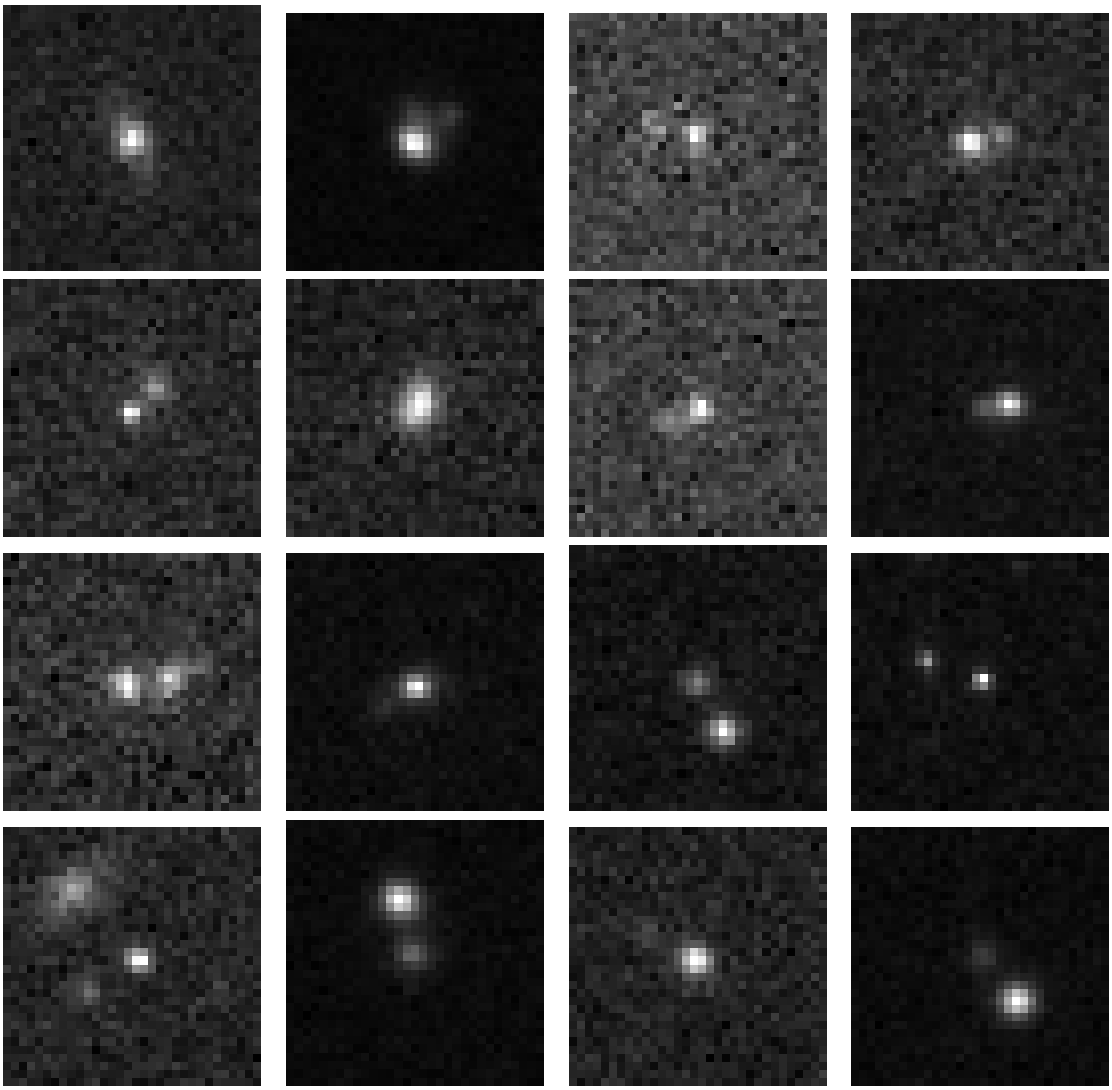

Figure 5.4: Sources from the A catalogue (continued) from left are, *first row*: 111525.6+013407, 111817.0+074558, 112646.0+07460, 113613.4+033841; *second row*: 115800.9+120439, 120320.2+053137, 120359.8+095419, 120749.2+082407; *third row*: 121405.1+010205, 122512.3+095420, 122726.9-001004, 123401.3+063215; *fourth row*: 123526.2+150807, 131625.2+114601, 133245.4+115238, 140939.6+074842

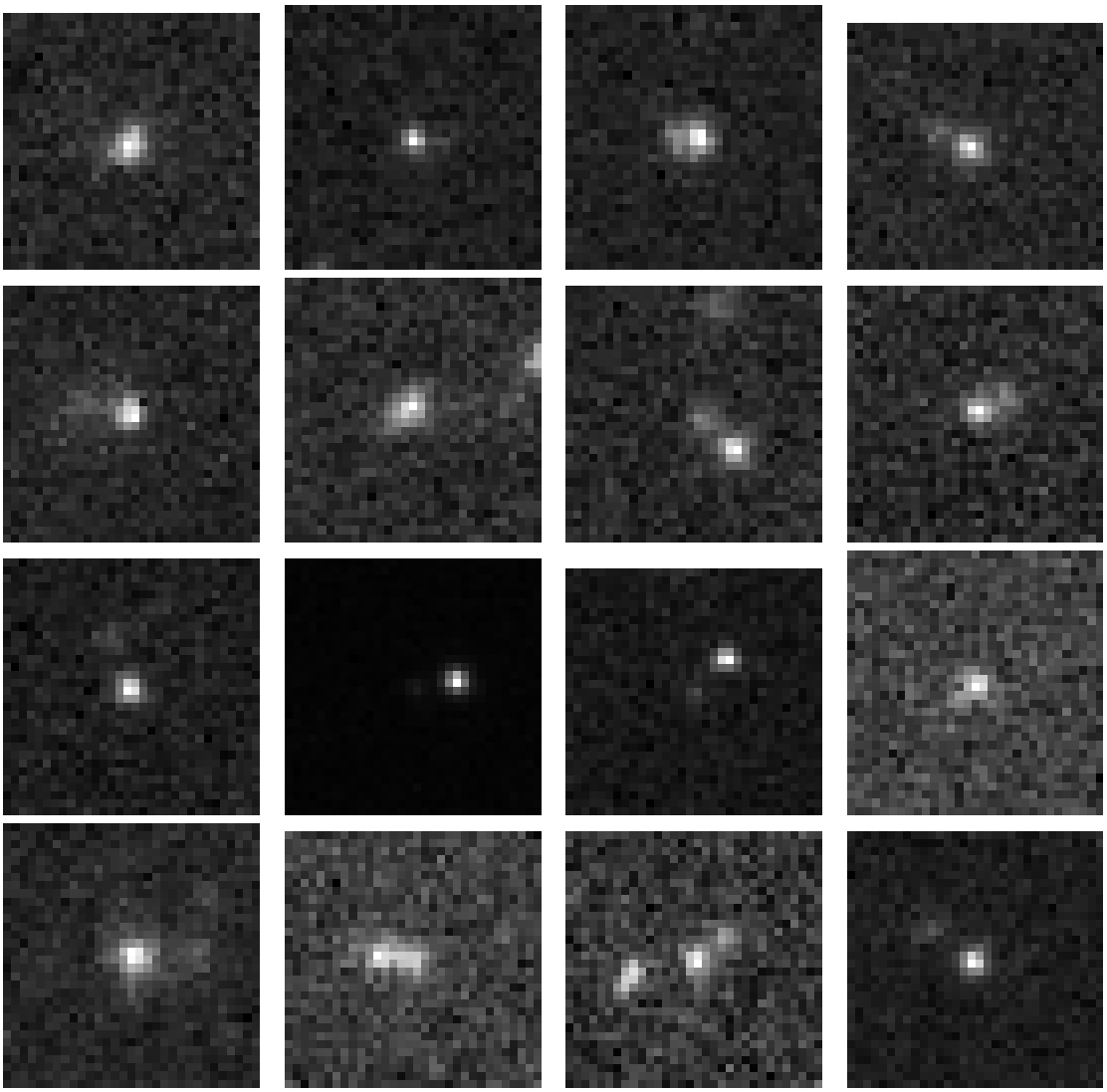

Figure 5.5: Sources from the A catalogue (continued) from left are, *first row*: 141637.4+003352, 141954.9+072255, 142526.5-004422, 142808.3+044826; *second row*: 142917.7+012059, 143058.8+003505, 143117.3+103939, 151505.1+041012; *third row*: 155446.5+093845, 214041.9-004359, 214958.2+001128, 215324.2+011437; *fourth row*: 215744.2+005304, 220906.9+004544, 221926.3-004613, 222417.3+011124

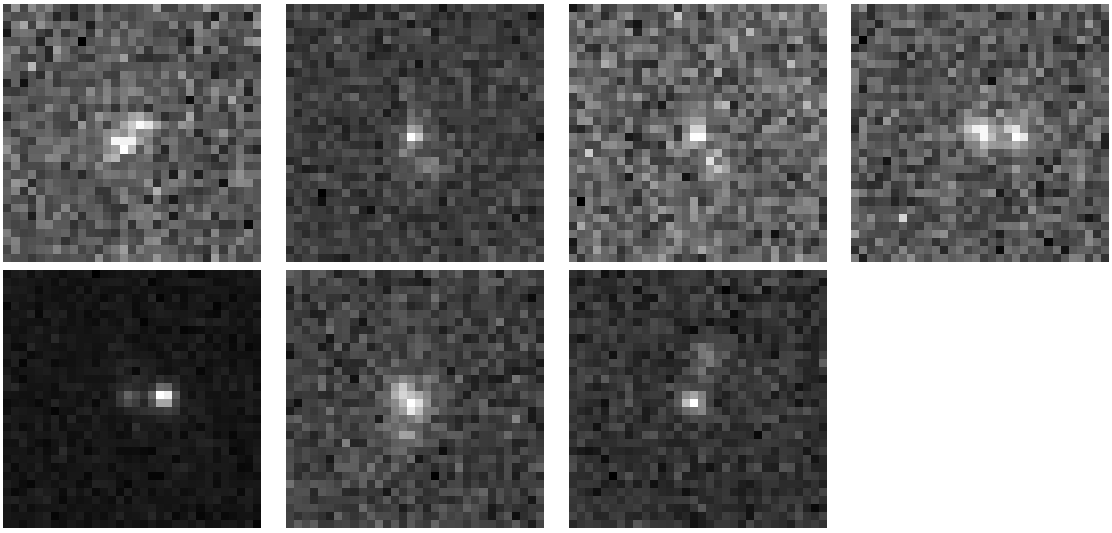

Figure 5.6: Sources from the A catalogue (continued) from left are, *first row*: 222929.5+010438, 225147.8+001641, 231148.5+004426, 232221.8+010733; *second row*: 233635.7-010734, 234623.4+010918, 235344.0+005217

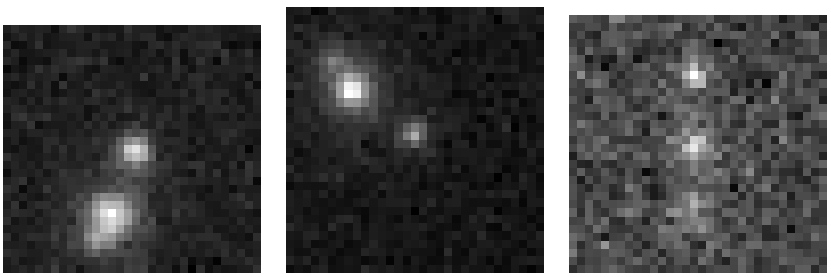

Figure 5.7: The 3 sources in the B catalogue: 092659.6+062327,094122.7+051822, 235643.4+001428

Chapter 6

Discussion

6.1 Survey Completeness

Figure 6.1 plots the image separation $\Delta\theta_i$ against flux ratio F_r for the simulated lenses (Chapter 4). The 36 positive identifications are shown by the green x's and the 13 false negatives are the black closed circles. This plot illustrates the completeness of this survey for lenses within the parameter range of $\Delta\theta_i \geq 1.0''$, and $F_r \leq 6$. However, at larger flux ratios ($F_r > 6$) the survey is not complete. 13 of the 19 simulated lenses within this range were rejected, suggesting a $\sim$ 46% probability in positively detecting a gravitational lens in this region of parameter space. However, figure 6.1 indicates that for $F_r > 6$ our survey is sensitive to lenses of separation $\sim 2.5''$. For this region of parameter space our survey is $\sim$ 60% complete. The plot also shows an apparent linear trend for the rejection of lenses at flux ratios between 8 to 15 with increasing image separation, which stops under $\sim 2.5''$.

The decrease in completeness at the higher flux ratios, is due to an increased uncertainty in the determination of the fainter image. This is true mainly for the *ug* wavebands, which generally had an error almost 3 times more than the *YHK* bands. The *ug* bands correspond to the wavelengths at which the galaxy have the least influence on brightness, making the determination of the maxima of the fainter image very difficult. This is especially true for sources with high flux ratios. Additionally, the *ug* bands have a PSF width of $1.4''$, lower than the $0.8''$ of the *YHK* bands. A combination of these effects decreases the detection capability for this survey at high flux ratios ($F_r > 6$), and smaller image separations. For the entire parameter space of $F_r \leq 15$ and $\Delta\theta_i \geq 1.0''$, the simulations suggest

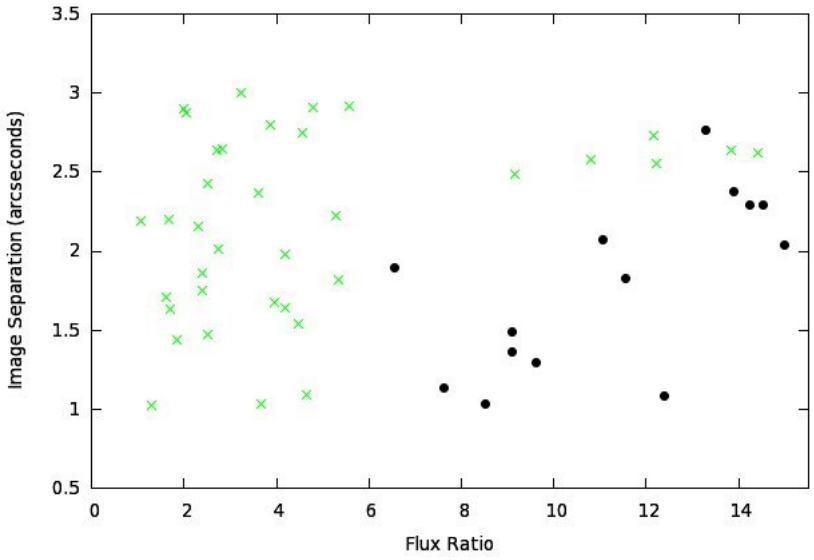

Figure 6.1: Image separation, $\Delta\theta_i$ against flux ratio F_r for the simulated lenses, obtained from the 4-step procedure. The positive identifications are shown by the green x's and the false negatives are the closed black circles.

an overall completeness of $\sim$ 74%

6.2 Lens Candidates

A histogram of the weighted image separations for all members of the P catalogue is shown in figure 6.2. The separations peak at $\sim 1.8''$, which is slightly higher than the value found by CLASS (Browne et al. 2003) and SQLS (Inada et al. 2008). The higher separation is due to the poor detection capability of this survey for combinations of high flux ratios and smaller separations (see Section 6.1). There are 3 sources (B list) with image separations $> 3.0''$, whose morphology shows evidence for more than two images (Figure 5.7). However, we are unable here to confirm this. A similar plot for the distribution of the flux ratios is given in figure 6.3. Although unremarkable, one noticeable feature is the increase of candidates between ratios of 10 and 15, following a sharp decline. It is possible that based upon the results of the simulations (Sections 4.3 and 6.3), these sources may be false positives. However, further analysis is needed.

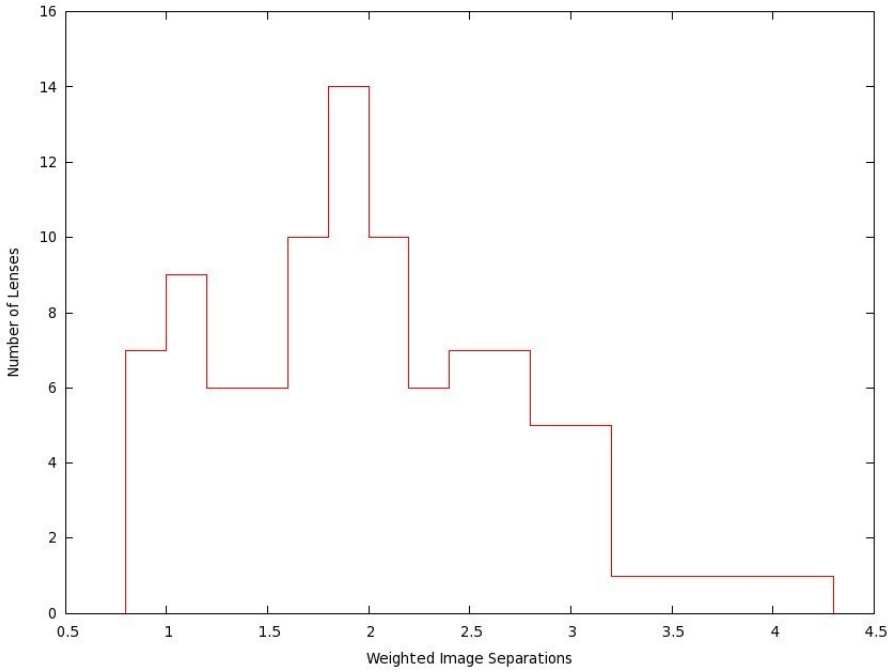

Figure 6.2: Distribution of the separation of the 90 lens candidates from the P catalogue. The smallest separation is $0.8''$, which is the limit of the survey. The units on the x-axis is arcseconds.

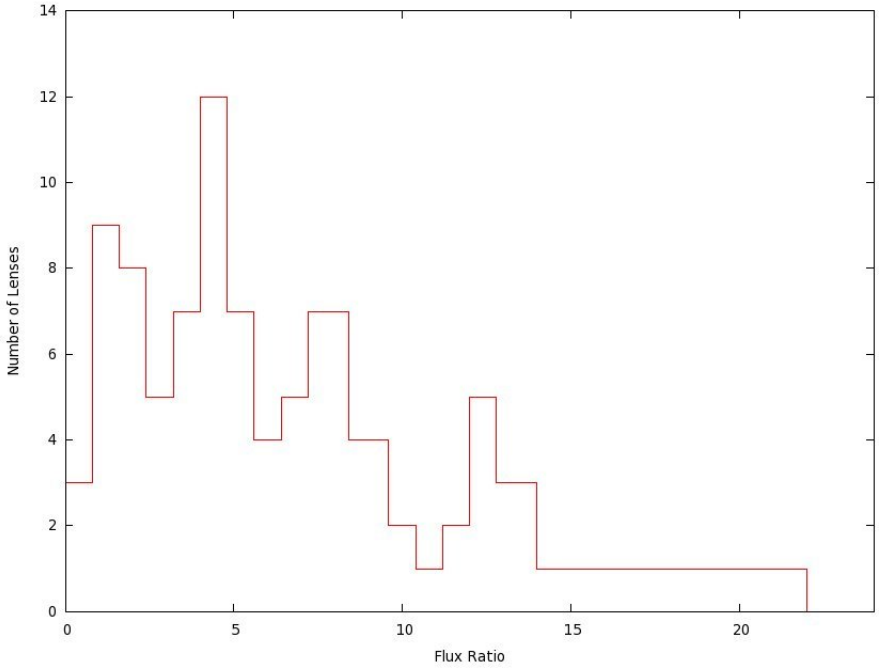

Figure 6.3: Distribution of the flux ratios of the 90 lens candidates from the P catalogue.

6.3 Comparison with Simulations

Figure 6.4 plots $\Delta\theta_i$ against F_r for the 90 members of the P catalogue. The A list sources are given by the red "+", and the 3 B list sources are the grey filled triangles ($\triangle$). Figure 6.5, shows figure 6.4 over plotted with figure 6.1. As expected from the last section, most of the lens candidates are within $F_r < 6$. The figure also shows that as F_r increases the number of candidates decreases greatly, until $F_r \sim 23$. There are quite a few lensed candidates that are beyond the flux ratio of 10. In addition, 5 lenses lie beyond the range explored by the simulations (i.e. $F_r > 15$). Although we cannot fully reject any of these candidates, any sources near or below the line (see Figure 6.6), that describes the apparent trend of the rejected lenses, will be regarded with suspicion.

As expected with any survey, there are false positives in our survey. To estimate the amount of false positives in our survey we looked at the population of known sources i.e. the 8 known lenses and the 10 known non-lenses. Of the 10 known non-lenses , 4 were in the C list and are hence rejected. This leaves 6 known non-lenses , from the original 28 in the final list of gravitational lens candidates. This suggests that $\sim$ 21% of "non-lensed" objects are classified as potential lens candidates, by our method. Also out of 14 *most probable lens candidates*, 6 are known to be "non-lensed" sources, which suggests a false-positive rate of $\sim$ 43%. Based upon this we can say that $\sim$ 50 sources in the P catalogue may be new gravitational lenses.

Figure 6.7, plots $\Delta\theta_i$ against F_r for the 8 known lenses (pink open squares) and 6 false positives (blue asterisks) along with figures 6.4 and 6.5. Here we see no pattern that corresponds to the false positives, as they are well mixed with the known lenses, positive simulation detections and the rejected simulated lenses.

6.4 Comparison to Other Surveys

Figure 6.8 compares the P catalogue against the lensed systems discovered by the CLASS/JVAS (Myers et al. 2003), and the SQLS (Inada et al. 2008, 2010) surveys. The CLASS lenses are the blue filled squares and the SQLS lenses are the black filled circles, and the blue asterisks.

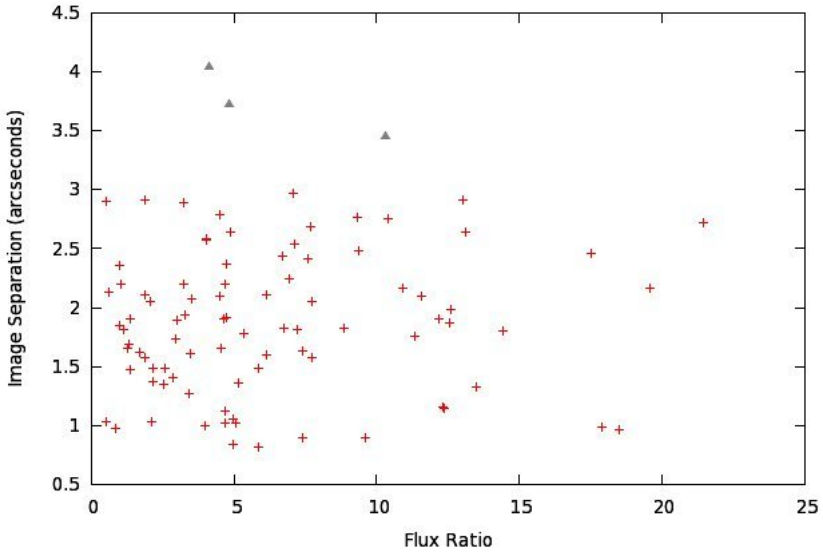

Figure 6.4: Image separation, $\Delta\theta_i$ against flux ratio F_r for the 90 sources in the P catalogue of possible gravitational lens candidates. The A list sources are given by the red "+", and the 3 B list sources are the grey filled triangles ($\triangle$).

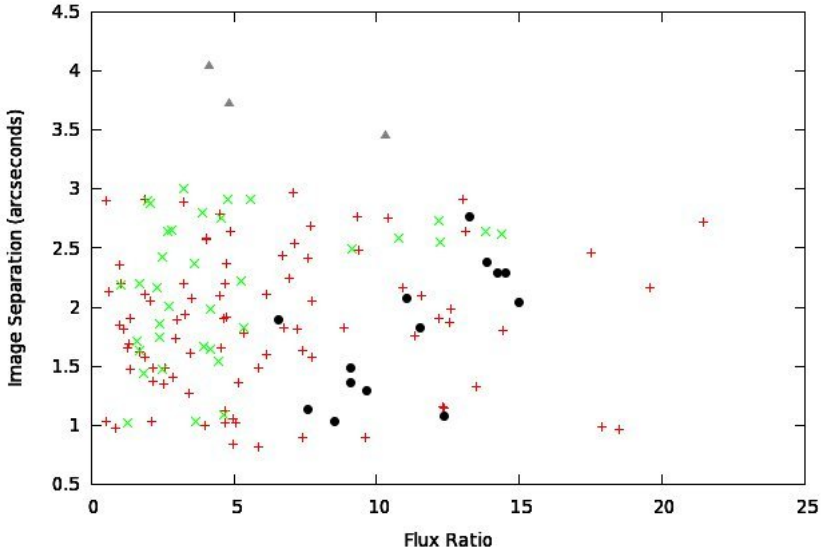

Figure 6.5: Combination plot of the P catalogue (Figure 6.4) and the simulated lenses (Figure 6.1). The colours, symbols and axes have the same meaning as Figures 6.1 and 6.4

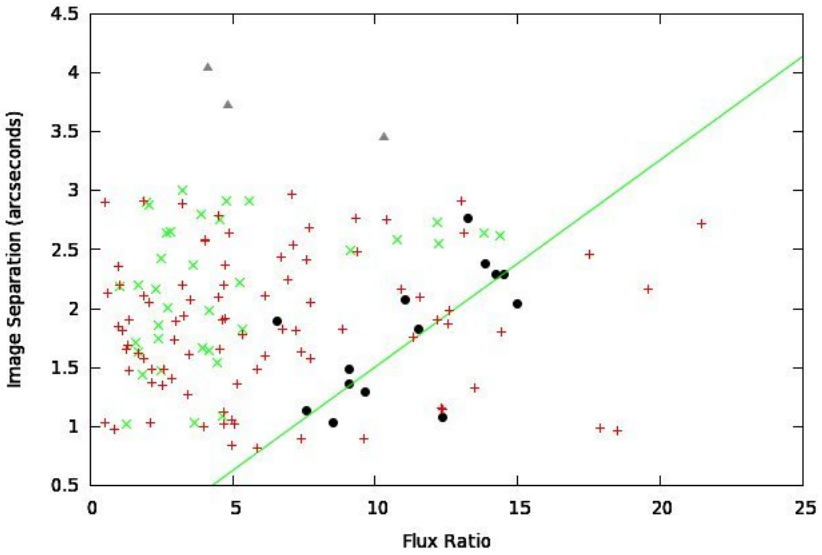

Figure 6.6: Same plot as Figure 6.5, with a linear description of the rejected simulated lenses (filled black circles). All candidates near or under this line will have a lower probability of being a lensed system.

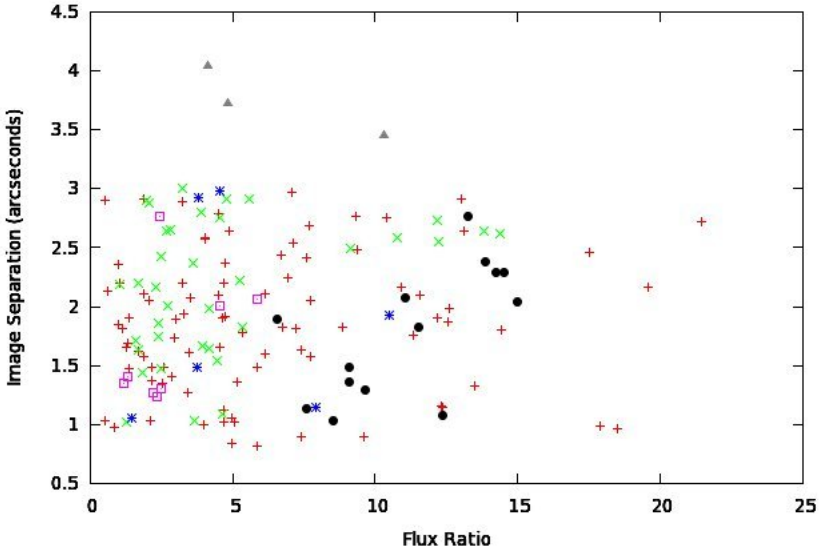

Figure 6.7: Plot showing the 8 known SQLS lenses in our survey (pink open squares), and the 6 false positives (blue asterisks), along with the points from Figures 6.4 and 6.5.

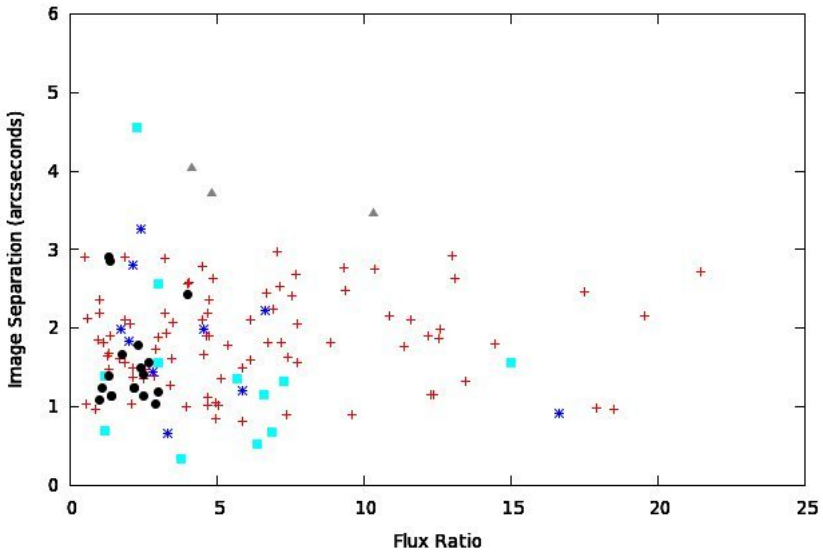

Figure 6.8: Comparison of the P catalogue with lenses from the CLASS/JVAS (filled blue squares, Browne et al. (2003)) and SQLS survey (open pink squares, Inada et al. (2008, 2010)).

6.4.1 CLASS

The CLASS is a well defined statistical sample of gravitational lenses under a flux ratio of 10, and is complete for $\Delta\theta_i > 0.3''$ (Browne et al. 2003). CLASS/JVAS found a total of 22 lenses, of which 12 are shown in figure 6.8. Most of the lenses are within the range $0.3'' < \Delta\theta_i < 3.0''$, while one lens is at $\Delta\theta_i > 3.0''$, which is assumed to be "cluster assisted" (Browne et al. 2003). 2 of the B list candidates are close to the parameters of the CLASS "cluster assisted" lens, which supports their inclusion into the list of possible gravitational lenses. Although this is not all the CLASS lenses, figure 6.8 clearly shows that for $\Delta\theta_i > 0.8''$, our survey observes systems similar to the CLASS lenses. Another important comparison is the maximum flux ratios. The one lens at $F_r \sim 15$, is from the JVAS and not considered as part of the CLASS well defined statistical sample. Considering that the CLASS survey restricted itself to $F_r \leq 10$, a comparison with the P catalogue candidates at $F_r > 10$ cannot be made. However, Browne et al. (2003) estimated a miss of $\sim 37\%$ due to this criteria.

The differential source counts for g-band quasars (Croom et al. 2009) roughly follows the differential source counts for radio quasars (McKean et al. 2007). Therefore, we can use the estimated lensing rates from the CLASS survey to estimate the expected number of lenses from our survey. Browne et al. (2003)

found a lensing rate of $10^{-2.8}$ which indicates that of a sample of 24,869 quasars, $\sim$ 40 would be lensed sources. CLASS/JVAS discovered 6 lenses with $\Delta\theta_i > 0.8''$, which is $\sim$ 27% of the total lenses found. If we take the CLASS/JVAS survey to be a true representation of the lens population, then our survey is expected to discover $\sim$ 30 new gravitational lenses within the image separation range $0.3'' < \Delta\theta_i < 3.0''$, and $F_r \leq 10$.

6.4.2 SQLS

Figure 6.8 plots the gravitational lenses discovered by the SQLS survey. The lenses represented by the black filled circles are 17 lenses from the SQLS statistical surveys (Inada et al. 2008, 2010), while the blue asterisks are the lenses that were found by the SQLS, but were rejected from the statistical sample (see Inada et al. (2008) for the reasons for rejection). We include them since we are interested in comparing all lenses that were discovered by the SQLS.

The SQLS statistical sample are mainly lenses with low flux ratios (i.e. $F_r < 4$), and are within the range $1.0'' < \Delta\theta_i < 3.0''$. This is within the parameter space indicated by our simulations that our survey is most sensitive to. Thus our survey would increase the range of parameter space explored by the SQLS. Based on Figure 6.8, we can see that the candidates presented in this survey, both follows the SQLS survey and serves as an extension of the SQLS. However, the SQLS survey used redshift as a selection criteria while it was not in our survey.

A lensing rate of $10^{-3.3}$ was found for the SQLS by Inada et al. (2008). This suggests that from our parent population of 24,869 sources, we would expect to detect $\sim$ 12 gravitational lensed sources, within $1.0'' < \Delta\theta_i < 3.0''$ and $F_r < 4$

6.5 Applications of this Survey

Generally most gravitational lensed surveys, especially the very large ones tend to be very time consuming. The most extreme case was CLASS, which took approximately 6 years for the observations (1993-1999), the summary papers were published in 2003, and the last lens discovery paper in 2005. SQLS also took a number of years to be completed ($\sim$ 6 yrs), and similarly SLACS. This is generally due to their adopted methodologies, which aims to efficiently reduce the false positives. However, the two survey, multi-wavelength gravitational lens detection method described in this thesis is expected to be far less time consuming

and very efficient at reducing the false positives. Such methods would allow the investigator to investigate a far larger parent population, and hence detect larger samples of gravitational lenses. It is far too early to compare the success of this survey to CLASS, SLACS and SQLS, as the 90 sources are yet to be observed.

Due to the multi-wavelength nature of this method would prove to be a very useful and efficient method to detect gravitational lenses with the upcoming Large Synoptic Survey Telescope (LSST[1]; LSST Science Collaborations et al. (2009)). The LSST will produce a 6-band ($ugrizY$) wide-field deep astronomical survey of over 20,000 square degrees of the southern sky using an 8.4-meter ground-based telescope. With the capabilities of the LSST, it is very likely that the method described here will detect much more gravitational lens candidates faster than any other survey within a wider range of parameter space. The LSST is set to be completed in 2012, with full survey operations in 2018.

[1] www.lsst.org/lsst

Chapter 7

Summary

A multi-wavelength method for detecting gravitational lenses have been presented. This method utilises a combination of two separate surveys, covering 8 colour (wavelength) bands; SDSS (*ugriz*) and UKIDSS (*ugriz*) aimed at effectively reducing the false positive population. The inverse relation of image separation to colour for gravitational lenses, discovered by Jackson et al. (2009) was the basis of this method. From an initial source population of 24 896, 461 were selected via morphological criteria, which was further reduced to 113 using the inverse relation method. Of the 113 sources, 87 were found to be within the image separation range, $0.8'' < \Delta\theta_i < 3.0''$ and were selected as *most probable gravitational lenses*. An additional 3 sources with $\Delta\theta_i > 3.0''$, were also included in the list.

The method was successful in identifying 8 out of 9 known gravitational lenses, indicating a $\sim$ 89% probability of positively identifying a gravitational lens. The lenses that was rejected, was due to an unaccounted increase in its brightness at the infrared bands. However, 6 out of 28 sources that were rejected by the SQLS survey as possible gravitational lenses, were selected by our method. This suggests a $\sim$ 27% probability of our method in selecting a source that is not a lens (false positive rate).

To determine the level of completeness, the inverse relation method was tested on simulated lenses. Simulated lenses were generated to "mimic" the lenses that are most likely detected by our method i.e. a blue lensed quasar with a red lens elliptical galaxy at a typical redshift of 0.5. The simulations focused on the completeness for two parameters; image separation, $\Delta\theta_i$ and flux ratio, F_r. 49 lenses were simulated within the parameter space $1.0'' < \Delta\theta_i < 3.0''$ and

$F_r < 15$. We can conclude that our survey is complete for lenses of image separation $> 1.0''$ and $F_r < 6$, but is insensitive to low separation lenses at high flux ratios.

Comparing to the CLASS survey, our survey is expected to miss $\sim 27\%$ of lenses due to the limit of $\Delta\theta_i > 0.8''$. With the expected lensing rates from the CLASS and SQLS surveys, we expect that 12 to 30 of our final list of candidates to be new gravitational lenses. This will only be certain following observations of the 90 sources with the Keck telescope, which are being planned for later in the year. If successful, this new method of detecting gravitational lenses, will be very important for the upcoming 8.4 m, 6 band ($ugrizY$) Large Synoptic Survey Telescope (LSST).

Bibliography

Adelman-McCarthy J.K., et al., 2008a, ApJS, 175, 297

Adelman-McCarthy J.K., et al., 2008b, ApJS, 175, 297

Auger M.W., Treu T., Bolton A.S., Gavazzi R., Koopmans L.V.E., Marshall P.J., Bundy K., Moustakas L.A., 2009, ApJ, 705, 1099

Bade N., Siebert J., Lopez S., Voges W., Reimers D., 1997, A&A, 317, L13

Bartelmann M., Schneider P., 2001, Phys. Rep., 340, 291

Bolton A.S., Burles S., Schlegel D.J., Eisenstein D.J., Brinkmann J., 2004, AJ, 127, 1860

Bolton A.S., Burles S., Koopmans L.V.E., Treu T., Moustakas L.A., 2006, ApJ, 638, 703

Bolton A.S., Burles S., Koopmans L.V.E., Treu T., Gavazzi R., Moustakas L.A., Wayth R., Schlegel D.J., 2008a, ApJ, 682, 964

Bolton A.S., Treu T., Koopmans L.V.E., Gavazzi R., Moustakas L.A., Burles S., Schlegel D.J., Wayth R., 2008b, ApJ, 684, 248

Browne I.W.A., et al., 2003, MNRAS, 341, 13

Cabanac R.A., et al., 2007, A&A, 461, 813

Carilli C.L., et al., 2002, ApJ, 575, 145

Casali M., et al., 2007, A&A, 467, 777

Chae K., 2003, MNRAS, 346, 746

Chae K., Chen G., Ratra B., Lee D., 2004, ApJL, 607, L71

Chiba M., Yoshii Y., 1999, ApJ, 510, 42

Chwolson O., 1924, Astron. Nachr., 221, 329

Comerford J.M., Meneghetti M., Bartelmann M., Schirmer M., 2006, ApJ, 642, 39

Condon J.J., Cotton W.D., Greisen E.W., Yin Q.F., Perley R.A., Taylor G.B., Broderick J.J., 1998, AJ, 115, 1693

Corless V.L., Dobke B.M., King L.J., 2008, MNRAS, 387, 803

Croom S.M., et al., 2009, MNRAS, 399, 1755

Dalal N., Kochanek C.S., 2002, ApJ, 572, 25

Djorgovski S., Davis M., 1987, ApJ, 313, 59

Dobke B.M., King L.J., Fassnacht C.D., Auger M.W., 2009, MNRAS, 397, 311

Dressler A., 1987, ApJ, 317, 1

Dyson F., Eddington A., Davidson C., 1920, Mem. R. Astron. Soc., 62, 291

Einstein A., 1911, Ann. Phys. (Leipzig), 35, 898

Einstein A., 1916, Ann. Phys. (Leipzig), 49, 769

Einstein A., 1922, Vier Vorlesungen über Relativitätstheorie. Vieweg, Braunschweig, Germany

Einstein A., 1936, Science, 84, 506

Falco E.E., Gorenstein M.V., Shapiro I.I., 1985, ApJL, 289, L1

Fassnacht C.D., Moustakas L.A., Casertano S., Ferguson H.C., Lucas R.A., Park Y., 2004, ApJL, 600, L155

Faure C., et al., 2008, ApJS, 176, 19

Ferreras I., Saha P., Williams L.L.R., Burles S., 2008, In J. Davies & M. Disney, ed., IAU Symposium, vol. 244 of IAU Symposium, pp. 206–215

Fort B., Prieur J.L., Mathez G., Mellier Y., Soucail G., 1988, A&A, 200, L17

Fukugita M., Futamase T., Kasai M., 1990, MNRAS, 246, 24P

Gavazzi R., Treu T., Rhodes J.D., Koopmans L.V.E., Bolton A.S., Burles S., Massey R.J., Moustakas L.A., 2007, ApJ, 667, 176

Gavazzi R., Treu T., Koopmans L.V.E., Bolton A.S., Moustakas L.A., Burles S., Marshall P.J., 2008, ApJ, 677, 1046

Gorenstein M.V., Shapiro I.I., Falco E.E., 1988, ApJ, 327, 693

Gregg M.D., Becker R.H., White R.L., Helfand D.J., McMahon R.G., Hook I.M., 1996, AJ, 112, 407

Gregory P.C., Scott W.K., Douglas K., Condon J.J., 1996, ApJS, 103, 427

Griffiths R.E., et al., 1994, ApJL, 435, L19

Hambly N.C., et al., 2008, MNRAS, 384, 637

Hennawi J.F., et al., 2006, AJ, 131, 1

Hewett P.C., Warren S.J., Leggett S.K., Hodgkin S.T., 2006, MNRAS, 367, 454

Hodgkin S.T., Irwin M.J., Hewett P.C., Warren S.J., 2009, MNRAS, 394, 675

Hogg D.W., Blandford R., Kundic T., Fassnacht C.D., Malhotra S., 1996, ApJL, 467, L73+

Huchra J., Gorenstein M., Kent S., Shapiro I., Smith G., Horine E., Perley R., 1985, AJ, 90, 691

Inada N., et al., 2003, AJ, 126, 666

Inada N., et al., 2006, AJ, 131, 1934

Inada N., et al., 2008, AJ, 135, 496

Inada N., et al., 2010, AJ, 140, 403

Jackson N., Ofek E.O., Oguri M., 2008, MNRAS, 387, 741

Jackson N., Ofek E.O., Oguri M., 2009, MNRAS, 398, 1423

Johnston D.E., et al., 2003, AJ, 126, 2281

King L.J., Browne I.W.A., Marlow D.R., Patnaik A.R., Wilkinson P.N., 1999, MNRAS, 307, 225

Kinney A.L., Calzetti D., Bohlin R.C., McQuade K., Storchi-Bergmann T., Schmitt H.R., 1996, ApJ, 467, 38

Kochanek C.S., 1996, ApJ, 466, 638

Kochanek C.S., Lawrence C.R., 1990, AJ, 99, 1700

Kochanek C.S., White M., 2001, ApJ, 559, 531

Kochanek C.S., Mochejska B., Morgan N.D., Stanek K.Z., 2006, ApJL, 637, L73

Koopmans L.V.E., the CLASS collaboration, 2001, PASA, 18, 179

Koopmans L.V.E., Treu T., Bolton A.S., Burles S., Moustakas L.A., 2006, ApJ, 649, 599

Lawrence A., et al., 2007, MNRAS, 379, 1599

LSST Science Collaborations, et al., 2009, preprint (astro-ph/0912.0201)

Lynds R., Petrosian V., 1986, In Bulletin of the American Astronomical Society, vol. 18 of Bulletin of the American Astronomical Society, p. 1014

Maoz D., Rix H., Gal-Yam A., Gould A., 1997, ApJ, 486, 75

Marshall P.J., Hogg D.W., Moustakas L.A., Fassnacht C.D., Bradač M., Schrabback T., Blandford R.D., 2009, ApJ, 694, 924

McGreer I.D., et al., 2010, AJ, 140, 370

McKean J.P., Browne I.W.A., Jackson N.J., Fassnacht C.D., Helbig P., 2007, MNRAS, 377, 430

McMahon R., Irwin M., Hazard C., 1992, GEMINI Newsletter Royal Greenwich Observatory, 36, 1

Mitchell J.L., Keeton C.R., Frieman J.A., Sheth R.K., 2005, ApJ, 622, 81

Moustakas L.A., et al., 2007, ApJL, 660, L31

Myers S.T., et al., 2003, MNRAS, 341, 1

Narayan R., Bartelmann M., 1996, preprint (astro-ph/9606001)

Narayan R., White S.D.M., 1988, MNRAS, 231, 97P

Oguri M., 2006, MNRAS, 367, 1241

Oguri M., 2007, ApJ, 660, 1

Oguri M., Keeton C.R., Dalal N., 2005, MNRAS, 364, 1451

Oguri M., et al., 2004, ApJ, 605, 78

Oguri M., et al., 2006, AJ, 132, 999

Oguri M., et al., 2008, AJ, 135, 512

Paczynski B., 1987, Nature, 325, 572

Patnaik A.R., Browne I.W.A., Wilkinson P.N., Wrobel J.M., 1992, MNRAS, 254, 655

Pindor B., 2005, ApJ, 626, 649

Pindor B., Turner E.L., Lupton R.H., Brinkmann J., 2003, AJ, 125, 2325

Pindor B., et al., 2006, AJ, 131, 41

Ratnatunga K.U., Griffiths R.E., Ostrander E.J., 1999, AJ, 117, 2010

Refsdal S., 1964, MNRAS, 128, 307

Riechers D.A., Walter F., Brewer B.J., Carilli C.L., Lewis G.F., Bertoldi F., Cox P., 2008, ApJ, 686, 851

Riess A., et al., 2005, Astrophys. J., 627, 579

Rusin D., Kochanek C.S., 2005, ApJ, 623, 666

Rusin D., et al., 2003, ApJ, 587, 143

Saha P., Coles J., Macciò A.V., Williams L.L.R., 2006, ApJL, 650, L17

Schneider D.P., et al., 2005, AJ, 130, 367

Schneider D.P., et al., 2007, AJ, 134, 102

Schneider P., Kochanek C.S., Wambsganss J., 2006, Gravitational Lensing: Strong, Weak and Micro., Saas-Fee Advanced Courses, Volume 33. Springer-Verlag Berlin Heidelberg, 2006

Scoville N., et al., 2007a, ApJS, 172, 1

Scoville N., et al., 2007b, ApJS, 172, 150

Soldner J., 1801, Berliner Astronomisches Jahrbuch, 1804, 161

Soucail G., Fort B., Mellier Y., Picat J.P., 1987, A&A, 172, L14

Soucail G., Mellier Y., Fort B., Cailloux M., 1988, A&AS, 73, 471

Suyu S.H., Marshall P.J., Blandford R.D., Fassnacht C.D., Koopmans L.V.E., McKean J.P., Treu T., 2009, ApJ, 691, 277

Suyu S.H., Marshall P.J., Auger M.W., Hilbert S., Blandford R.D., Koopmans L.V.E., Fassnacht C.D., Treu T., 2010, ApJ, 711, 201

Treu T., Koopmans L.V.E., 2002, ApJ, 575, 87

Treu T., Koopmans L.V.E., 2004, ApJ, 611, 739

Treu T., Koopmans L.V., Bolton A.S., Burles S., Moustakas L.A., 2006, ApJ, 640, 662

Treu T., Gavazzi R., Gorecki A., Marshall P.J., Koopmans L.V.E., Bolton A.S., Moustakas L.A., Burles S., 2009, ApJ, 690, 670

Turner E.L., 1990, ApJL, 365, L43

Turner E.L., Ostriker J.P., Gott III J.R., 1984, ApJ, 284, 1

Walsh D., Carswell R.F., Weymann R.J., 1979, Nature, 279, 381

Wambsganss J., 1998, Living Reviews in Relativity, 1

Warren S.J., Hewett P.C., Lewis G.F., Moller P., Iovino A., Shaver P.A., 1996, MNRAS, 278, 139

Warren S.J., Iovino A., Hewett P.C., Shaver P.A., 1998, MNRAS, 299, 1215

Warren S.J., Lewis G.F., Hewett P.C., Møller P., Shaver P., Iovino A., 1999, A&A, 343, L35

Willis J.P., Hewett P.C., Warren S.J., Dye S., Maddox N., 2006, MNRAS, 369, 1521

York D.G., et al., 2000a, AJ, 120, 1579

York D.G., et al., 2000b, AJ, 120, 1579

York T., Jackson N., Browne I.W.A., Wucknitz O., Skelton J.E., 2005, MNRAS, 357, 124

Zepf S.E., Moustakas L.A., Davis M., 1997, ApJL, 474, L1+

Zwicky F., 1937a, Phys. Rev. Lett., 51, 290

Zwicky F., 1937b, Phys. Rev. Lett., 51, 679